

# Causal Discovery in Nonlinear Dynamical Systems using Koopman Operators

Adam Rupe,<sup>1</sup> Derek DeSantis,<sup>2</sup> Craig Bakker,<sup>1</sup> Parvathi Kooloth,<sup>1</sup> and Jian Lu<sup>1</sup>

<sup>1</sup>*Pacific Northwest National Laboratory*

<sup>2</sup>*Los Alamos National Laboratory*

(Dated: October 15, 2024)

We present a theory of causality in dynamical systems using Koopman operators. Our theory is grounded on a rigorous definition of causal mechanism in dynamical systems given in terms of flow maps. In the Koopman framework, we prove that causal mechanisms manifest as particular flows of observables between function subspaces. While the flow map definition is a clear generalization of the standard definition of causal mechanism given in the structural causal model framework, the flow maps are complicated objects that are not tractable to work with in practice. By contrast, the equivalent Koopman definition lends itself to a straightforward data-driven algorithm that can quantify multivariate causal relations in high-dimensional nonlinear dynamical systems. The coupled Rössler system provides examples and demonstrations throughout our exposition. We also demonstrate the utility of our data-driven Koopman causality measure by identifying causal flow in the Lorenz 96 system. We show that the causal flow identified by our data-driven algorithm agrees with the information flow identified through a perturbation propagation experiment. Our work provides new theoretical insights into causality for nonlinear dynamical systems, as well as a new toolkit for data-driven causal analysis.

## I. INTRODUCTION

For many complex dynamical systems, there is a disconnect between the governing equations and system behaviors due to a web of strong nonlinear dependencies [1]. Simulations that numerically solve the governing equations are just a starting point for understanding the complex behaviors that emerge. Causal discovery is a potent form of analysis to identify and quantify the detailed processes that give rise to these behaviors [2, 3]. The standard statistical framework for causal inference [4], however, is insufficient for identifying causal relations in nonlinear dynamical systems. While tools specifically designed for causal discovery in dynamical systems have shown promise, some notable gaps remain in their theoretical foundations and algorithmic implementation. In this work we introduce a novel framework for causal discovery in nonlinear dynamical systems using Koopman operators to address these shortcomings.

Essentially all of the statistical approaches to causal inference assume that causal flow is unidirectional, represented by an acyclic causal graph, and many assume linear causal relationships. These assumptions do not hold for nonlinear dynamical systems. The unidirectional assumption cannot account for feedbacks, which are ubiquitous in complex nonlinear systems. In climate science, for example, a central question is how the Earth system responds to forcing [5]. One can simulate various input forcings and record the resulting responses, but it is not necessarily straightforward to follow all of the processes that lead from the input forcing to the output response. This is particularly the case when there are

feedbacks between subprocesses that amplify or attenuate signals propagating through component interactions. The standard approach to identify the effects of feedbacks in system responses to forcing is to compare forcing responses in the actual system with responses in a ‘counterfactual’ system in which the feedback process is removed [6]. This approach requires high-fidelity simulations of the system behaviors, and even then it is not always clear how to properly “turn off” or remove the feedback process because of the interconnectedness of the various sub-processes [7].

In addition, the lack of linear superposition makes it very difficult for statistical methods to disentangle the effects of individual mechanisms that interact and intertwine. Together with strong coupling and feedbacks, we require global holistic approaches to parse the complex behaviors generated by nonlinear dynamical systems. For example, how can the clouds of Jupiter simultaneously support apparently random chaotic motion together with coherent structures, like the Great Red Spot, that spontaneously emerge as islands of order in the sea of turbulence? We know the fundamental physics sufficiently well that we can produce such behaviors in simulation, but it is not at all clear how this happens from inspecting the governing equations.

In response to these difficulties, researchers have developed bespoke causal inference methods specifically for nonlinear dynamical systems. The existing toolkit falls largely into two categories, with methods based on either information flows or delay-coordinate embeddings. Information flows [8–10] generalize the early approaches of Wiener [11] and Granger [12], who argued that  $Y(t)$  has a causal

effect on  $X(t)$  if past observations of  $Y(t)$  help to better predict the future evolution of  $X(t)$ . The other class of methods [13–15] utilize the insight of attractor reconstruction using past observations [16, 17], called delay-coordinate embeddings in this context. The idea being that if  $X(t)$  and  $Y(t)$  belong to the same chaotic dynamical system, then their delay embeddings will reconstruct the same geometric object—namely the attractor of their dynamical system. Transfer entropy [18] and convergent cross mapping [15] are the main representatives of information flows and delay embedding methods, respectively. Both have their strengths and limitations, as outlined in e.g. Ref. [3].

Here, we introduce a rigorous first-principles approach that is complementary to information flows and delay embedding methods. Our theory is based on Koopman operators [19] that provide a *global linearization* of general nonlinear dynamics. Rather than track the nonlinear evolution of individual system states, Koopman theory shifts perspectives to the linear evolution of system *observables*—scalar functions of the system state. The global linearization of Koopman operators provides the ability to disentangle the complex web of interactions in general nonlinear systems without restrictive assumptions like small forcing or remaining near equilibrium.

The power of Koopman operators and their global linearization enables the following advancements for causal discovery in nonlinear dynamical systems. i) We provide a rigorous definition of causal mechanism for dynamical systems, adapting the definition given by the structural causal model framework [20]. ii) This definition highlights the importance of the *time scale* of causal relations in dynamical systems, which is often neglected in other approaches to causality in dynamical systems. iii) We prove an equivalent definition of causal mechanism in terms of Koopman operators that lends itself to a simple data-driven algorithm to quantify causal relations. Whereas most other algorithms for dynamical systems identify causal relations between two univariate time series, our method can naturally accommodate multivariate relations in high-dimensional systems.

Our Koopman theory of causality unfolds as follows. In Section II we introduce the necessary background and notation for dynamical system flow maps and Koopman operators. Here we define dynamical system components, the analog of variables like  $X$  and  $Y$  above, over which dynamical causal relations are defined. Section III introduces our definition of causality and causal mechanisms for dynamical systems and its formulation in the Koopman framework. We prove that the two definitions are equivalent. In Section IV we introduce our data-driven

measures to quantify the degree of causal influence and demonstrate them using the coupled Rössler system. Finally, Section V provides a detailed case study of the Lorenz 96 system and its causal flows driven by advection. We show that our data-driven Koopman measure identifies a spatilally-asymmetric causal wave that agrees with the wave of information flow identified using a perturbation propagation experiment. We close with a discussion in Section VII.

## II. PRELIMINARIES

### A. Dynamical Systems

Dynamical systems theory describes how a system evolves over time. Mathematically, the system state is given as a point in a *phase space*  $\Omega$ . The phase space often comes equipped with additional topological or measure theoretic structure depending on the system described. For all the examples we consider in this work,  $\Omega$  is the standard Euclidean space  $\mathbb{R}^N$ , though the results hold equally well for  $N$ -manifolds. Because we will deal almost exclusively with vector quantities, we will not use any notation (e.g.  $\vec{\omega}$ ) to distinguish vector quantities from scalar quantities. Variables should be considered as vectors unless otherwise stated.

Time-evolution is given by a semigroup of *flow maps*—functions that map the phase space back to itself  $\{\Phi^t : \Omega \rightarrow \Omega\}_{t \in \mathcal{T}}$ . Flow map semigroups are applicable to both discrete time dynamics, with  $\mathcal{T} = \mathbb{N}$ , and continuous time,  $\mathcal{T} = \mathbb{R}_{\geq 0}$ . All of our examples are in continuous time, but our formalism is given generally in terms of flow maps that can be in discrete or continuous time. For continuous time, we will assume additional structure on the flow maps, namely that they are differentiable (and thus also continuous) [21].

For discrete-time dynamical systems, such as iterated maps [22, 23], a generator function  $\Phi : \Omega \rightarrow \Omega$  gives the unit-step evolution as

$$\omega(n+1) = \Phi(\omega(n)) .$$

The semigroup elements  $\{\Phi^m\}_{m \in \mathbb{N}}$  are then given through  $m$ -fold composition, so that, e.g. for  $m = 2$ ,  $\omega(n+2) = \Phi^2(\omega(n)) = [\Phi \circ \Phi](\omega(n))$ .

For continuous time, we consider differential dynamical systems in which  $\Phi$  specifies the time-derivative of the system state  $\omega \in \Omega$

$$\dot{\omega} = \frac{d}{dt}\omega = \Phi(\omega) .$$

The flow maps  $\Phi^t$  are generated from  $\Phi$  through time

integration, so that

$$\omega(t) = \Phi^t(\omega) = \omega + \int_0^t \Phi(\omega(\tau)) d\tau .$$

For both discrete and continuous time, the time-evolution of the system state  $\{\omega(t) = \Phi^t(\omega)\}_{t \in \mathcal{T}}$  is called an *orbit*, with initial condition  $\omega$ , or simply the orbit of  $\omega$ . Note that orbits are functions of both time and initial condition, the latter of which is implicit in our notation. That is,  $\omega(t) = \Phi^t(\omega)$  is interpreted as the state at time  $t$  starting from initial state  $\omega$ . To be explicit, this is equivalent to designating the initial state as  $\omega_0$  and writing  $\omega(t, \omega_0) = \Phi^t(\omega_0)$ . We use the simplified notation to avoid excessive clutter.

As in discrete time, the flow maps form a semigroup through composition so that

$$\begin{aligned} \omega(t+t') &= \Phi^{t+t'}(\omega) = [\Phi^t \circ \Phi^{t'}](\omega) \\ &= \Phi^t(\Phi^{t'}(\omega)) = \Phi^t(\omega(t')) . \end{aligned}$$

The infinitesimal generator of the semigroup of flow maps is given by  $\Phi$ , the time-derivative of the system states,

$$\Phi(\omega) = \lim_{\tau \rightarrow 0^+} \frac{1}{\tau} (\Phi^{t+\tau}(\omega) - \Phi^t(\omega)) = \frac{d}{dt} \Phi^t(\omega)|_{t=0} .$$

For simplicity, we restrict ourselves to *autonomous* dynamical systems for which  $\Phi$  does not have explicit time dependence.

## B. System Components

Our causal theory concerns how one ‘part’ of a dynamical system may or may not influence the dynamics of another ‘part’. We now formalize the idea of ‘parts’ of a dynamical system. Recall that we consider state spaces  $\Omega$  such that system states  $\omega \in \Omega$  are  $N$ -dimensional vectors. We refer to each scalar element of  $\omega$ , and equivalently each dimension of  $\Omega$ , as a **degree of freedom**. Thus, for the system  $\Omega = \mathbb{R}^N$ , there are  $N$  degrees of freedom. Our interest is in causal relations between distinct subsets of degrees of freedom, which we call *components*.

**Definition II.1.** Consider a dynamical system with an  $N$ -dimensional phase space and hence  $N$  degrees of freedom. The degrees of freedom may be partitioned into system **components**—non-overlapping subsets of degrees of freedom. We denote the partitioning of phase space into component subspaces as  $\Omega = \Omega_1 \times \Omega_2 \times \dots \times \Omega_L$ , with  $\omega_i \in \Omega_i$ , and write  $\omega = [\omega_1 \ \omega_2 \ \dots \ \omega_L]^\top$ .

Note that the partitioning of degrees of freedom into components is mathematically arbitrary and depends on the context of the problem and causality questions being asked. For example, if  $\omega = [x \ y \ z]^\top \in \mathbb{R}^3$ , we can partition into  $L = 2$  components with, e.g.,  $\omega_1 = [x \ y]^\top$  and  $\omega_2 = [z]$ . We can also choose, e.g.,  $\omega_1 = [y]$  and  $\omega_2 = [x \ z]^\top$  as a valid  $L = 2$  component partition.

**Example 1.** To be concrete, we now introduce the model system that will guide our exposition, two **coupled Rössler oscillators**:

$$\begin{aligned} \dot{x}_1 &= -\varphi_1 y_1 - z_1 \\ \dot{y}_1 &= \varphi_1 x_1 + a y_1 + c_1 (y_2 - y_1) \\ \dot{z}_1 &= b + z_1 (x_1 - d) \\ \\ \dot{x}_2 &= -\varphi_2 y_2 - z_2 \\ \dot{y}_2 &= \varphi_2 x_2 + a y_2 + c_2 (y_1 - y_2) \\ \dot{z}_2 &= b + z_2 (x_2 - d) , \end{aligned} \tag{1}$$

with constants  $a, b, c_i, \varphi_i \in \mathbb{R}$ . This is a six-dimensional system,  $\Omega = \mathbb{R}^6$ , with a natural partitioning into two components  $\omega = [\omega_1 \ \omega_2]^\top$  where each component has three degrees of freedom  $\omega_j = [x_j \ y_j \ z_j]^\top$ . Note that the coupling between the systems in this case is linear, through the  $y_i$  degrees of freedom only, with coupling constants  $c_i$ . Also, Rössler oscillators are weakly nonlinear, with a single quadratic nonlinearity in the  $z$  variable dynamics.

## C. Reproducing Kernel Hilbert Spaces

The Koopman operator, defined below, is a type of map between function spaces. The most natural type of function space for data analysis are the reproducing kernel Hilbert spaces. We will need to leverage properties about reproducing kernel Hilbert spaces throughout this work—in particular product spaces of reproducing kernel Hilbert spaces.

Let  $\Omega$  be a non-empty set. A collection of functions  $\mathcal{F}$  mapping  $\Omega$  to  $\mathbb{C}$  is said to be a *reproducing kernel Hilbert space (RKHS)* if

- $\mathcal{F}$  is endowed with the vector space structure over  $\mathbb{C}$ :  $(f + g)(x) = f(x) + g(x)$
- $\mathcal{F}$  is equipped with an inner product  $\langle \cdot, \cdot \rangle$ , with which  $\mathcal{F}$  becomes a Hilbert space (complete inner product space)
- The evaluation functionals  $E_\omega : \mathcal{F} \rightarrow \mathbb{C}$  via  $E_\omega(f) = f(\omega)$  are bounded ( $\sup_{\|f\| \leq 1} |E_\omega(f)| < \infty$ ) for all  $\omega \in \Omega$

By the Riesz representation theorem, there exists functions  $k_\omega \in \mathcal{F}$  such that  $E_\omega(f) = \langle f, k_\omega \rangle$ . These functions are called *the reproducing kernel at  $\omega$* . The *kernel function*  $K : \Omega \times \Omega \rightarrow \mathbb{C}$  defined by  $K(\omega, \omega') := \langle k_{\omega'}, k_\omega \rangle = k_{\omega'}(\omega)$  uniquely defines a RKHS by the Moore-Aronszajn theorem [24]. We denote the RKHS associated to the kernel  $K$  by  $\mathcal{H}(K)$ . It is known that the reproducing kernels are dense in the Hilbert space:

$$\mathcal{H}(K) = \overline{\text{span}_{\omega \in \Omega} \{k_\omega\}}$$

where the overline denotes closure in the norm of  $\mathcal{H}(K)$ .

Our Koopman causality theory will require reproducing kernels associated to (arbitrary) subdivisions of the phase space  $\Omega$  into components. Suppose that there are  $L$  components,  $\Omega = \Omega_1 \times \Omega_2 \times \dots \times \Omega_L$ . Let  $K_i$  be a kernel function defined over  $\omega_i$ . Then for  $\omega = [\omega_1 \ \omega_2 \ \dots \ \omega_L]^\top \in \Omega$ , one can define the tensor product of functions  $[f_1 \otimes f_2 \otimes \dots \otimes f_L](\omega) := f_1(\omega_1)f_2(\omega_2) \dots f_L(\omega_L)$  where  $f_i \in \mathcal{H}(K_i)$ . The tensor product space  $\mathcal{H}(K_1) \otimes \dots \otimes \mathcal{H}(K_L)$  is a Hilbert space, with inner product

$$\langle \otimes f_i, \otimes g_i \rangle = \prod \langle f_i, g_i \rangle_{\mathcal{H}(K_i)}$$

This Hilbert space consists of functions that are limits of sums of these elementary tensors  $\otimes f_i$ . One may define the *tensor product kernel*  $K : \Omega \times \Omega$  by

$$K(\omega, \omega') = K_1(\omega_1, \omega'_1) \dots K_L(\omega_L, \omega'_L)$$

It is well known that  $\mathcal{H}(K)$  is naturally isomorphic to  $\mathcal{H}(K_1) \otimes \dots \otimes \mathcal{H}(K_L)$  [24]. Note that the kernel at a point  $\omega'$  for the tensor product kernel is expressed as a tensor product of the individual kernels:

$$k_{\omega'}(\omega) = \prod_{i=1}^L K_i(\omega_i, \omega'_i) = \prod_{i=1}^L k_{\omega'_i}(\omega_i)$$

That is,  $k_{\omega'} = \otimes_{i=1}^L k_{\omega'_i}$ . See Appendix A for an example using random Fourier features.

Given that data comes as discrete point-evaluations of functions, RKHS serve as the natural Hilbert spaces for data driven analysis of dynamical systems [25]. While not strictly a requirement, we will simplify the theory discussed in this work by restricting our attention to RKHS's. Any function space  $\mathcal{F}$  is thus assumed to be a RKHS unless otherwise specified.

#### D. Koopman Operators

As we will elaborate on further below, nonlinearity in the dynamics  $\Phi$  makes it very challenging to

track causal dependencies among components of the system state  $\omega$  over time. Over the last decade, Koopman theory [19] has emerged as a powerful new approach that provides a *global linearization* of arbitrary dynamical systems, even if  $\Phi$  is highly nonlinear. This is in contrast to standard linear stability analysis provided by the Hartman-Grobman theorem [26] which states that a dynamical system is locally linear near a hyperbolic fixed point so that the system state evolves linearly in a small neighborhood around the fixed point.

Of course, if  $\Phi$  is nonlinear, the evolution of the system state  $\omega$  cannot be linear everywhere. Global linearization in Koopman theory is achieved by taking a different perspective. Rather than analyze the evolution of individual system states, Koopman theory analyzes the evolution of system *observables*—scalar functions of the system states  $f : \Omega \rightarrow \mathbb{C}$ , with  $f$  as an element of some function space  $\mathcal{F}$ . The evolution of observable functions, given by Koopman operators, is linear for all dynamical systems, as long as the function space  $\mathcal{F}$  is a vector space. The price that is paid, however, is that the linear evolution of observables generically occurs in infinite dimensions. Throughout, we will assume that our observables arise as functions in an RKHS  $\mathcal{F}$  over the phase space  $\Omega$ .

The action of a *Koopman operator*  $\mathcal{K}^t : \mathcal{F} \rightarrow \mathcal{F}$  on an observable  $f \in \mathcal{F}$  yields a time-shifted observable, denoted as  $f_t \in \mathcal{F}$ , that is given by the composition of  $f$  with the flow map  $\Phi^t$  [27]

$$f_t(\omega) = [\mathcal{K}^t f](\omega) := [f \circ \Phi^t](\omega) = f(\omega(t)) . \quad (2)$$

As mentioned,  $\mathcal{K}^t$  is a linear operator on  $\mathcal{F}$ , since for all  $\alpha \in \mathbb{C}$  and  $f, g \in \mathcal{F}$

$$\mathcal{K}^t(\alpha f + g)(\omega) = \alpha f(\omega(t)) + g(\omega(t)) = \alpha \mathcal{K}^t f(\omega) + \mathcal{K}^t g(\omega)$$

Koopman operators inherit the semigroup structure of the flow maps:  $\mathcal{K}^{t+t'} = \mathcal{K}^t \mathcal{K}^{t'}$ . The action of the Koopman semigroup  $\{\mathcal{K}^t\}_{t \in \mathcal{T}}$  on a given observable  $f_0$  produces an orbit in function space  $\{f_t = \mathcal{K}^t f_0\}_{t \in \mathcal{T}}$ , analogous to orbits of systems states in the original system. We emphasize that this is an orbit of functions, which can be tricky to work with. However, the evaluation of an observable orbit at a given system state  $\omega(0)$  yields a scalar time series, given equivalently as

$$\{f_t(\omega(0))\}_{t \in \mathcal{T}} = \{f_0(\omega(t))\}_{t \in \mathcal{T}} . \quad (3)$$

These observable time series are the objects we work with for data-driven approximation of Koopman operators, discussed in more detail shortly.

Koopman operators over RKHS satisfy the particularly nice property of being bounded. A linear operator  $T : \mathcal{H} \rightarrow \mathcal{K}$  mapping between Hilbert

spaces  $\mathcal{H}$  and  $\mathcal{K}$  is said to be *bounded* if there exists some constant  $M$  such that  $\|Tf\| \leq M\|f\|$  for all  $f \in \mathcal{H}$ . It is well known that for linear operators, being bounded is equivalent to being continuous. A Koopman operator whose action on a RKHS stays inside the RKHS is automatically bounded:

**Theorem II.1.** *Let  $\mathcal{F}$  be a RKHS, and  $\mathcal{K}^t$  satisfy that  $\mathcal{K}^t f \in \mathcal{F}$  for all  $f \in \mathcal{F}$  ( $\mathcal{K}^t : \mathcal{F} \rightarrow \mathcal{F}$ ). Then  $\mathcal{K}^t$  is bounded (continuous).*

See Appendix C 1 for the proof.

### E. Finite-Dimensional Approximation: Dynamic Mode Decomposition

The *dynamic mode decomposition* (DMD) family of algorithms [28, 29] provides a matrix approximation  $K^t$  of the Koopman operator  $\mathcal{K}^t$  from data using a least-squares regression. The matrix  $K^t$  converges to a Galerkin projection of  $\mathcal{K}^t$  on a finite-dimensional subspace of  $\mathcal{F}$  in the infinite data limit [28, 29]. Let  $\Psi = [\psi_1 \ \psi_2 \ \cdots \ \psi_M]^\top$  be a *dictionary* of scalar-valued observables in  $\mathcal{F}$  and  $\mathcal{F}_\Psi = \text{span}(\Psi) \subset \mathcal{F}$  the finite-dimensional Hilbert subspace spanned by the dictionary  $\Psi$ . The *Galerkin projection* of  $\mathcal{K}^t$  to the finite subspace  $\text{span}(\Psi) := \mathcal{F}_\Psi \subset \mathcal{F}$  is the unique linear operator  $K^t : \mathcal{F}_\Psi \rightarrow \mathcal{F}_\Psi$  that satisfies

$$\langle \psi_j, \mathcal{K}^t \psi_i \rangle = \langle \psi_j, K^t \psi_i \rangle, \quad \text{for all } \psi_i, \psi_j \in \Psi .$$

We assume that data is taken from a measurable dynamical system  $(\Omega, \Sigma, \mu, \Phi)$  and collected into  $D$  pairs  $\{(\omega(n), \omega^t(n))\}_D$  of system states  $\omega(n)$  and their  $t$ -shifts  $\omega^t(n) := \Phi^t(\omega(n)) = \omega(n+t)$ . Each  $\omega(n)$  is an  $N$ -dimensional vector. All of our examples below utilize continuous-time dynamical systems with a fixed sampling interval  $\delta t$ , and the  $t$ -shifts are given as integer multiples of  $\delta t$ .

The data points  $\{(\omega(n), \omega^t(n))\}_D$  are collected into data matrices, with the state vectors  $\omega(n)$  in  $\Omega \in \mathbb{R}^{N \times D}$  and their  $t$ -shifts  $\omega^t(n)$  in  $\Omega^t \in \mathbb{R}^{N \times D}$ :

$$\Omega = \begin{bmatrix} \omega(n_1) & \omega(n_2) & \cdots & \omega(n_D) \\ \vdots & \vdots & & \vdots \end{bmatrix} \quad (4)$$

and

$$\Omega^t = \begin{bmatrix} \omega^t(n_1) & \omega^t(n_2) & \cdots & \omega^t(n_D) \\ \vdots & \vdots & & \vdots \end{bmatrix}, \quad (5)$$

respectively.

Using the dictionary functions  $\psi_i : \Omega \rightarrow \mathbb{R}$  in  $\Psi$ , we create observable, or “boosted”, data matrices

$$\Psi = \begin{bmatrix} \Psi(\omega(n_1)) & \cdots & \Psi(\omega(n_D)) \\ \vdots & & \vdots \end{bmatrix} \quad (6)$$

and

$$\Psi^t = \begin{bmatrix} \Psi(\omega^t(n_1)) & \cdots & \Psi(\omega^t(n_D)) \\ \vdots & & \vdots \end{bmatrix}, \quad (7)$$

where

$$\Psi(\omega(n)) = [\psi_1(\omega(n)) \ \cdots \ \psi_M(\omega(n))]^\top \in \mathbb{R}^M,$$

and  $\Psi, \Psi^t \in \mathbb{R}^{M \times D}$ . Each column of  $\Psi$  is an  $M$ -dimensional vector of point-evaluations of each of the  $M$  functions  $\psi_i$  in the dictionary  $\Psi$  at the point  $\omega(n)$ .

Dynamic mode decomposition seeks the best-fit matrix that evolves the dictionary functions, based on their point-evaluations from the time shifts in the dataset. The DMD matrix  $K$  minimizes the error

$$\begin{aligned} & \sum_{n=1}^D \|[\mathcal{K}^t \Psi](\omega(n)) - K^t \Psi(\omega(n))\|^2 \\ &= \sum_{n=1}^D \|[\Psi \circ \Phi^t](\omega(n)) - K^t \Psi(\omega(n))\|^2 \quad (8) \\ &= \sum_{n=1}^D \|\Psi(\omega^t(n)) - K^t \Psi(\omega(n))\|^2 . \end{aligned}$$

The error is equivalent to the Frobenius norm  $\|\Psi^t - K^t \Psi\|_F^2$ .

The least-squares solution to Eq. (8) is given as

$$K^t := \Psi^t \Psi^\dagger, \quad (9)$$

where  $\Psi^\dagger$  is the pseudoinverse of  $\Psi$ .

We have emphasized in Eq. (8) that the shifted observable data matrix  $\Psi^t$  is given by point-evaluations of the true action of the full Koopman operator  $\mathcal{K}^t$ . As the Koopman operator is defined in terms of composition with the system dynamics  $\Phi$ ,  $\Psi^t$  is created from the full system dynamics and all its complexity—including relevant causal interactions. Said another way, the approximation  $K^t$  does not involve any simplification of the underlying dynamics  $\Phi^t$ .

The DMD approximation  $K^t$  converges to the Koopman operator  $\mathcal{K}^t$  in the strong operator topology as  $D, M \rightarrow \infty$  [30].

### F. Random Fourier Feature Observables

In this work, we use random Fourier features [31] for our dictionary observables as they are simple, flexible, and effective. A *random Fourier feature dictionary*  $\Psi_{\text{RFF}}$  is simply a collection of  $M$  cosine functions,

$$\Psi_{\text{RFF}}(\omega) = \begin{bmatrix} \cos(\phi_1^\top \omega + b_1) \\ \cos(\phi_2^\top \omega + b_2) \\ \vdots \\ \cos(\phi_M^\top \omega + b_M) \end{bmatrix}, \quad (10)$$

where each frequency  $\phi_j$  is an  $N$ -dimensional random vector sampled from a specified distribution  $p(\phi)$  and  $b_j$  are uniformly-distributed random variables. Random Fourier features are seen as a Monte Carlo approximation to a positive-definite and shift-invariant kernel, with the distribution  $p(\phi)$  determining the kernel [31]. For example, random Fourier features with  $p(\phi)$  distributed as a spherical Gaussian approximate a Gaussian kernel. We utilize Gaussian  $p(\phi)$  with a diagonal covariance matrix for our random Fourier features in the numerical results below.

In Appendix A, we recall how random Fourier features approximate shift-invariant kernels and thus the RKHS defined by that kernel. We show that tensor products of random Fourier features are also random Fourier features. This allows us to use RFFs for component function spaces as well as full system function spaces.

### III. KOOPMAN THEORY OF CAUSALITY IN DYNAMICAL SYSTEMS

We now consider causality for nonlinear dynamical systems. First, we define necessary terms and the existence of causal relations in dynamical systems. We then briefly examine the difficulties of quantifying the degree of causal effects in nonlinear systems. This motivates us to formulate causality in the Koopman perspective of the evolution of system observables. The global linearization of observable dynamics makes quantifying causal effects much more tractable for nonlinear systems. We provide the theory of causality using Koopman operators, then give an operational algorithm based on DMD to quantify causal relations from data.

#### A. Causal Mechanism

To build our theory on solid foundations, we first must address the question: what is a *causal mechanism*? Theories of causal inference generally identify a causal mechanism through a *structural causal model* [4, 20]. A random variable  $X$  is assigned values according to its structural assignment:

$$X := m(\text{pa}(X), \epsilon_X), \quad (11)$$

where  $\text{pa}(X)$  are the causal “parents” of  $X$  and  $\epsilon_X$  is an IID random variable. The map  $m$  is interpreted as the causal mechanism of  $X$ , whose specific value is determined by some set of other variables,  $\text{pa}(X)$ , that are said to causally influence  $X$ . The noise term  $\epsilon_X$  summarizes all other factors not explicitly modeled, and all noise terms for the full system are assumed to be jointly independent. Conceptually, a variable  $Y$  is said to be a cause of a variable  $X$  if  $X$  can change in response to changes in  $Y$ .

Notice that time does not appear in the structural causal model in Eqn. (11). Typical causal questions addressed in the statistical framework, such as “Did the aspirin cause my headache to go away?” or “Does obesity shorten life?” [32], are not framed in terms of temporal evolution. To include sequential changes over time, statistical methods simply add time dependence to the variables but assume a time-invariance of the qualitative causal relationships [3]. This *causal stationarity* assumption means the functional form of causal mechanisms do not change over time, and thus neither do the causal parents.

As we will see, causal stationarity is not a reasonable assumption for nonlinear dynamical systems, particularly those with spatial extent. For spatially-extended systems with local interactions, causal influence spreads through the interactions at a finite rate. Therefore, *causal mechanisms can qualitatively change over different time scales*.

#### B. Causality in Dynamical Systems

We now adapt the notion of causal mechanism to dynamical systems using flow maps. Because the flow maps are fully parameterized by time, our definition reveals the importance of time scales for causal mechanisms and how they may qualitatively change over time. In addition, our definition highlights the difficulty of identifying causal relations in nonlinear dynamical systems—individual flow maps are complicated objects that generally do not have an interpretable closed-form analytical solution.

To properly define causal mechanisms for dynamical systems, we first require the following definition:

**Definition III.1.** Let  $\Omega = \Omega_1 \times \dots \times \Omega_L$  be a partition of a dynamical system  $(\Omega, \Phi)$ . Given an initial state  $\omega = [\omega_1 \dots \omega_L] \in \Omega$ , recall that the **orbit** of  $\omega$  is  $\{\omega(t) := \Phi^t(\omega)\}_{t \in \mathcal{T}}$ . We define the **component orbit**  $\omega_j(t)$  as

$$\omega_j(t) := P_j \omega(t) = P_j \Phi^t(\omega) \in \Omega_j, \quad (12)$$

where  $P_j$  is the coordinate projection of  $\omega$  onto component  $\omega_j \in \Omega_j$ .

The central question for the *existence* of a causal relationship in dynamics is whether the orbit of an “effect” component depends on the “cause” component. At first this seems limited to a bipartite analysis: e.g., the effect of component  $\Omega_j$  on component  $\Omega_i$ . We may, however, want to know the synergistic causal effects that, say, components  $\Omega_j$  and  $\Omega_k$  together have on component  $\Omega_i$ . Fortunately, our definition of components is sufficiently flexible to allow for such a multipartite analysis—we can simply combine  $\Omega_j$  and  $\Omega_k$  into a single component  $\Omega_j \times \Omega_k$ .

For the general exposition of our theory, we introduce the following definitions.

**Definition III.2.** Let  $(\Omega, \Phi)$  be a dynamical system. For causal analysis, we specify a fixed partition

$$\Omega = \Omega_C \times \Omega_E \times \Omega_R$$

of  $\Omega$  into a **cause component**  $\Omega_C$ , an **effect component**  $\Omega_E$ , and **remainder component**  $\Omega_R$ . The remainder component may or may not be empty.

**Example 2.** Consider the coupled Rössler oscillators in Example 1. We may be interested in the causal influence of component  $\omega_1 = [x_1 \ y_1 \ z_1]^\top$  on component  $\omega_2 = [x_2 \ y_2 \ z_2]^\top$ . In this case, we designate  $\Omega_C = \Omega_1$ ,  $\Omega_E = \Omega_2$ , and the remainder  $\Omega_R$  is empty. We may also be interested in more fine-grained details on the causal interaction. For example, the coupling between the two oscillators is through the  $y$  degrees of freedom, so we may want to know how much of the causal influence from  $\Omega_1$  to  $\Omega_2$  is carried by  $y_1$  versus by  $x_1$  and  $z_1$ . In both of these cases, we let  $\Omega_E = \Omega_2$ . In the first case we would have  $\Omega_C = \{y_1\}$  with  $\Omega_R = \{x_1, z_1\}$ , and in the second case  $\Omega_C = \{x_1, z_1\}$  with  $\Omega_R = \{y_1\}$ .

The example above emphasizes that the designation of cause and effect components  $\Omega_C$  and  $\Omega_E$  is arbitrary and depends on the causal questions being investigated. The subscripts  $C$  and  $E$  are replaced by numerical subscripts, as above, when specifying pre-defined components in a particular system under investigation.

With the cause, effect, and remainder components defined, we can now make precise the existence of causal relations in dynamical systems.

**Definition III.3.** Let  $\Omega = \Omega_E \times \Omega_C \times \Omega_R$  be defined as above. Fix a  $t > 0$  and consider the component flow  $P_E \Phi^t$  that is the mapping from a full system state initial condition to the ‘effect’ component  $\Omega_E$  at time  $t$

$$[\omega_E \ \omega_C \ \omega_R]^\top \mapsto \omega_E(t).$$

We say that  $\Omega_C$  **dynamically causally influences**  $\Omega_E$  **at time**  $t$  if  $\omega_E(t)$  depends on the initial  $\omega_C$ .

We denote this by  $\Omega_C \xrightarrow{t} \Omega_E$ . Otherwise,  $\Omega_C$  **does not dynamically causally influence**  $\Omega_E$  **at time**  $t$ , and we write  $\Omega_C \not\xrightarrow{t} \Omega_E$ .

If  $\Omega_C \xrightarrow{t} \Omega_E$  for any  $t \in \mathcal{T}$ , we say that  $\Omega_C$  **dynamically causes** component  $\Omega_E$ , and write  $\Omega_C \rightarrow \Omega_E$ . If for all  $t$  there is no causal influence, we say that  $\Omega_C$  **does not dynamically cause**  $\Omega_E$  and write  $\Omega_C \not\rightarrow \Omega_E$ .

**Remark 1.** The component flow maps  $P_E \Phi^t$  play the role of **causal mechanisms** in our dynamical systems theory, analogous to structural causal models, e.g., Eqn. (11). Like other causal inference frameworks, we say that component  $\Omega_C$  has a causal effect on  $\Omega_E$  if and only if  $\Omega_C$  appears in the causal mechanism for  $\Omega_E$ . As emphasized in the Introduction, however, the component flow maps are parameterized by the time scale  $t$  and, as we will see below, can qualitatively change over time.

**Remark 2.** Consider two components with  $\Omega = \Omega_1 \times \Omega_2 \times \Omega_R$ . If we have that either  $\Omega_2 \rightarrow \Omega_1$  or  $\Omega_1 \rightarrow \Omega_2$ , then  $\Omega_1$  and  $\Omega_2$  are necessarily components of the same dynamical system. If, on the other hand, we have that both  $\Omega_1 \not\rightarrow \Omega_2$  and  $\Omega_2 \not\rightarrow \Omega_1$ , then  $\Omega_1$  and  $\Omega_2$  are **independent** dynamical systems. Finally, if both  $\Omega_1 \rightarrow \Omega_2$  and  $\Omega_2 \rightarrow \Omega_1$ , we say there is a **dynamical feedback** between the components  $\Omega_1$  and  $\Omega_2$ .

While straightforward to define causality between components in dynamical systems, it is not as obvious how to quantify the *degree of causality* for nonlinear systems. The next example illustrates the issue.

**Example 3.** Consider the coupled Rössler system given in Eqn. (1) with the two components  $\Omega = \Omega_1 \times \Omega_2$ . If  $c_1 \neq 0$ , then  $\Omega_2 \rightarrow \Omega_1$  because the evolution of  $y_1$  depends on  $y_2$ . Similarly, if  $c_2 \neq 0$  then  $\Omega_1 \rightarrow \Omega_2$ . If both  $c_1 = c_2 = 0$ , then the two Rössler oscillators  $[x_1 \ y_1 \ z_1]^\top \in \Omega_1$  and  $[x_2 \ y_2 \ z_2]^\top \in \Omega_2$  are independent. If  $c_1$  and  $c_2$  are both nonzero, then there is a dynamical feedback between the two Rössler components of the joint coupled oscillator system.

Consider the case of  $c_1 \neq 0$  and  $c_2 = 0$ . It is clear from inspecting the equations of motion that  $\Omega_2 \rightarrow \Omega_1$  and  $\Omega_1 \not\rightarrow \Omega_2$ . For a specified set of parameters (with  $c_1 \neq 0$  and  $c_2 = 0$ ) in the coupled Rössler system, can we identify the degree to which  $\Omega_2 \rightarrow \Omega_1$ ? Given that Rössler oscillators are only (weakly) nonlinear in the  $z$  degree of freedom and the two Rössler systems are linearly coupled, we might expect the causal influence of  $\Omega_2$  on  $\Omega_1$  to scale with the coupling coefficient  $c_1$ .

To examine causal phenomenology of the coupled Rössler system and explore the interplay of nonlinearity in the oscillators with linear coupling between

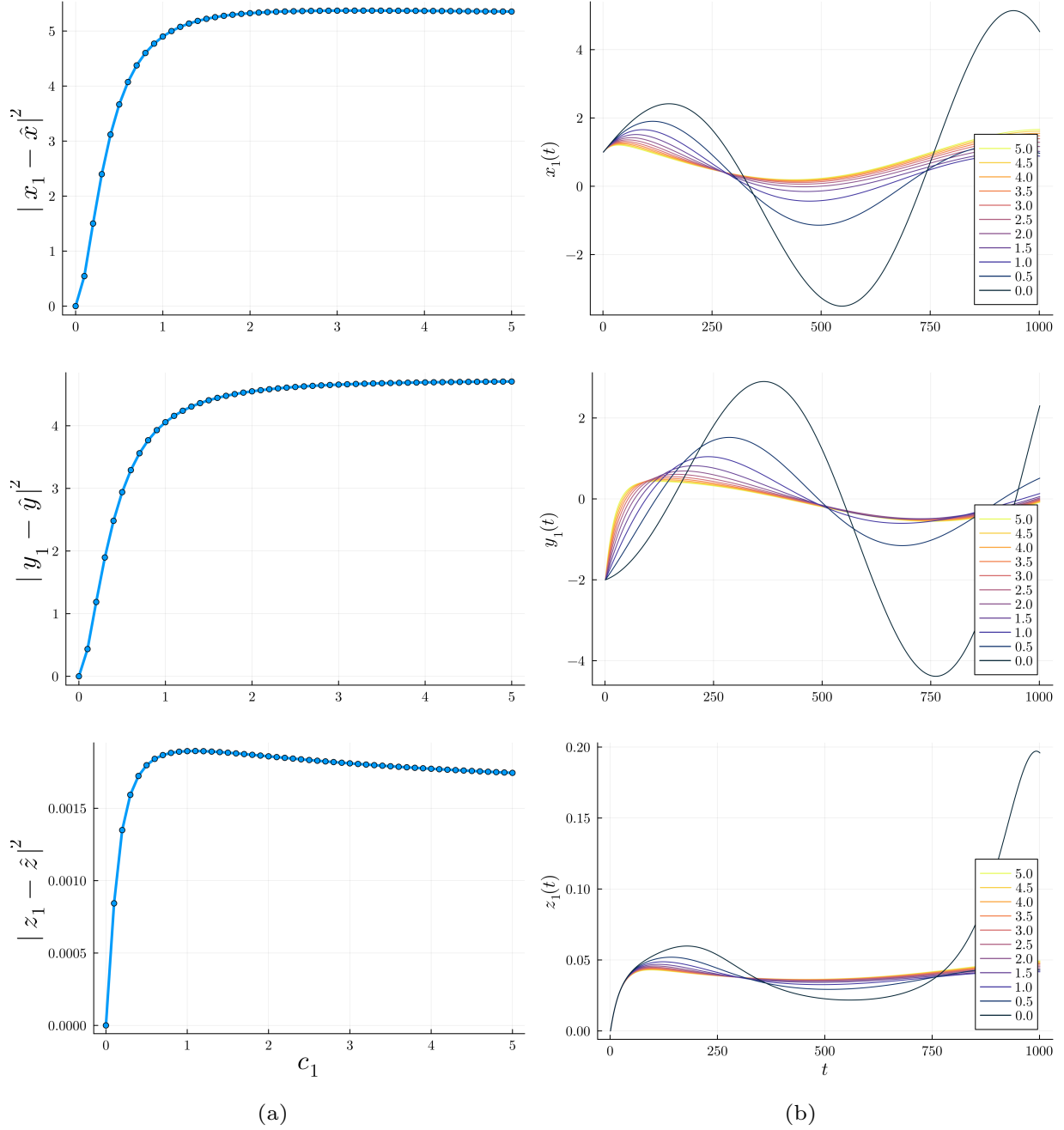


FIG. 1. Some causal phenomenology of the coupled Rössler oscillator system using a counterfactual causality measure. Column (a) shows causality from an asymmetrical system with  $\Omega_2 \rightarrow \Omega_1$  and  $\Omega_1 \not\rightarrow \Omega_2$ . Column (b) shows sample time series of each degree of freedom with increasing coupling constants  $c_1$ .

them, here we use the lens of counterfactuals. Because we are numerically simulating the system and have full control, we can simulate a counterfactual system that is an independent Rössler oscillator with identical parameters and initial conditions to  $\Omega_1$  in the coupled system. The counterfactual system gives

what the evolution of  $\Omega_1$  would have been if there were no causal influence from  $\Omega_2$ . We can thus define a *counterfactual measure of causality* by computing the mean-squared error between the evolution of  $\Omega_1$  and the counterfactual system:



$$\frac{1}{T} \sum_T \|\omega_1(t) - \hat{\omega}_1(t)\|^2, \quad (13)$$

where  $\hat{\omega}_1$  is the counterfactual (i.e., a copy of the original system but with  $c_1 = 0$ ). Here, we compare the orbits out to time  $T$  that is just below one Lyapunov time.

We note that this counterfactual measure is really only possible for systems which can be effectively simulated. It is not necessarily possible to compute in *every* simulation. It is simple here because the existence of the causal influence  $\Omega_2 \rightarrow \Omega_1$  is entirely controlled by whether  $c_1$  is zero or not. In more complicated simulations, like climate models, with many nonlinearly-coupled components, it is not straightforward to “turn off” causal influence as necessary to create the counterfactual model [7].

Figure 1 (a) shows the counterfactual causal measure of the  $\Omega_2 \rightarrow \Omega_1$  coupled Rössler system as a function of the coupling coefficient  $c_1$ . Each degree of freedom  $\{x_1, y_1, z_1\} \in \Omega_1$  is analyzed separately in each row. In all cases, we see that causal measure increases sharply as the coupling is first turned on, but quickly saturates to an asymptotic value. Therefore, it is only in the “weakly coupled” regime with small  $c_1$  that causality is proportional to the coupling constant. As coupling is increased further, it no longer contributes to differences in the orbits between the coupled system and the counterfactual independent system.

One may intuit that stronger coupling pushes the system to behave more erratically. Hence the saturation seen in Figure 1 (a) perhaps results from the orbits being pushed to the bounds of the attractor, which limits how far apart an orbit and its counterfactual can be. It turns out that the opposite is true: increased coupling to  $\Omega_2$  acts to stabilize the trajectories of  $\Omega_1$ . This is shown in Figure 1 (b), with sample orbits of each degree of freedom given for increasing values of the coupling constant  $c_1$ . As we see, the orbits with the largest variance are those with small coupling. The causality measure saturates because the orbits converge with increased coupling. Recall that  $c_1 = 0$  is the counterfactual case of no coupling.

This simple example, with weakly non-linear coupling completely controlled by a single parameter, illustrates the challenges of quantifying causality. While causal influence is, to some degree, controlled by the coupling constants in the coupled Rössler system, it cannot be directly quantified by the coupling constants alone. The effects of the linear coupling also interact with the nonlinearity of the Rössler oscillators. The situation is especially complicated in

the presence of feedbacks when both oscillators are coupled together, which we discuss in Appendix B.

### C. Causality in the Koopman Framework

For simple systems like the coupled Rössler oscillators, the existence of dynamical causal relations is obvious from inspection of the equations of motion—given that they are known. However, for complex systems like a coupled Earth system model, it is not necessarily so clear. More significantly, even for a simple system like the coupled Rössler oscillators with linear coupling and weak nonlinearity, quantifying the degree of causal influence is very challenging, as we have just demonstrated.

This motivates us to formulate dynamical causality in the Koopman framework. The global linearization in the dynamics of system and component observables turns out to be hugely beneficial for identifying and quantifying causal relations in nonlinear systems directly from data. First, we provide the equivalent of dynamical causality in terms of Koopman operators and flows in function space. The theory then suggests a data-driven algorithm based on DMD to quantify the degree of causal influence with a clear interpretation.

#### 1. Component observables and function space embeddings

Dynamical causality in the Koopman framework manifests as flows in function space. A key step then is to properly formulate the space of observables for individual components as closed subspaces of the function space for the joint dynamical system.

Let  $\Omega = \Omega_1 \times \dots \times \Omega_L$  be a partition of  $\Omega$ . For each component, let  $K_i$  be a kernel function of  $\Omega_i$ . We make the following assumption:

**Assumption:** We assume that for each  $i$ , the RKHS  $\mathcal{H}(K_i)$  contains the constant functions.

We now define the kernel  $K$  to be the tensor product kernel of  $K_i$ ,  $i = 1, \dots, L$ , and set  $\mathcal{F} = \mathcal{H}(K)$ . Note that by assumption,  $\mathcal{F}$  will contain functions which are constant on any arbitrary collection of components of  $\Omega$ . This facilitates the following definition:

**Definition III.4.** Let  $\Omega = \Omega_1 \times \dots \times \Omega_L$ ,  $K_i$ ,  $K$  and  $\mathcal{F}$  be as above. Given  $X \subset \{1, 2, \dots, L\}$ , let  $\Omega_X = \times_{j \in X} \Omega_j$ . We define  $\mathcal{F}_X$  to be the functions in  $\mathcal{F}$  which depend only on  $\Omega_X$ . That is,  $\mathcal{F}_X$  is the set of  $f \in \mathcal{F}$  such that  $f$  restricted to  $\Omega_{X^c}$  are constant.

**Lemma III.1.** *Let  $\Omega = \Omega_1 \times \dots \times \Omega_L$ ,  $K_i$ ,  $K$  and  $\mathcal{F}$  be as above. For each  $X \subset \{1, 2, \dots, L\}$ , we have that  $\mathcal{F}_X$  is a closed subspace in  $\mathcal{F}$ .*

See Appendix C 2 for the proof.

Each of the component subspaces  $\mathcal{F}_X$  contains all the information about observables on the space  $\Omega_X$ . The function space  $\mathcal{F}$  of the full system, on the other hand, contains all the observables on the full state space  $\Omega = \Omega_1 \times \dots \times \Omega_L$ . As  $\mathcal{F}_X$  are closed subspaces of  $\mathcal{F}$ , they themselves are (reproducing kernel) Hilbert spaces. We have the following connection between the spaces  $\mathcal{F}_X$  and the kernel function  $K$ :

**Proposition III.1.** *Let  $X \subset \{1, 2, \dots, L\}$ , and  $K_i$ ,  $\mathcal{F}_X$  be as above. Define the kernel function  $K_X : \Omega \times \Omega \rightarrow \mathbb{C}$  by*

$$K_X(\omega', \omega) := \prod_{j \in X} K_j(\omega'_j, \omega_j)$$

for all  $\omega, \omega' \in \Omega$ . Define the functions  $k_{X,\omega} : \Omega \rightarrow \mathbb{C}$  by  $k_{X,\omega}(\omega') = K_X(\omega', \omega)$ . Then

$$\mathcal{F}_X = \overline{\text{span}_{\omega \in \Omega} \{k_{X,\omega}\}}$$

See Appendix C 3 for the proof.

Therefore, the component kernel functions  $K_X$  define the component function subspaces  $\mathcal{F}_X = \mathcal{H}(K_X)$  through their reproducing kernels  $k_{X,\omega'}$ . The component reproducing kernels and function subspaces naturally compose to the full joint system through tensor products.

## 2. Existence of causal relations from Koopman operators

With the component observable function subspaces appropriately defined, we now turn to identifying the Koopman equivalent of the existence of dynamical causality. The central idea of our theory is that the existence and absence of dynamical causal relations produce distinct behaviors in the flow of functions in the observable space  $\mathcal{F}$ .

Recall from Eqn. (2) above that the action of a Koopman operator on an observable  $f \in \mathcal{F}$  gives a new function in  $f_t \in \mathcal{F}$  defined by the composition of  $f$  with the flow map  $\Phi^t$ . Therefore, the time-shifted function  $f_t$  inherits functional dependence from the flow map. Intuitively, if component  $\Omega_C$  has no causal influence on component  $\Omega_E$ , then the Koopman evolution of functions  $\mathcal{F}_C$  that initially only depend on  $\Omega_C$  should be indifferent to values of  $\omega_E \in \Omega_E$ . From Definition III.3, if  $\Omega_C \not\rightarrow \Omega_E$ , then the component flow map for  $\Omega_E$  does not depend on  $\Omega_C$  and so the action of Koopman operators on functions in  $\mathcal{F}_E$  will

inherit this functional independence. We now make these ideas precise.

**Definition III.5.** Let  $(\Omega, \Phi)$  be a dynamical system as above. Consider a fixed partition

$$\Omega = \Omega_C \times \Omega_E \times \Omega_R$$

of  $\Omega$  into a ‘cause’, ‘effect’, and ‘residual’ components respectively. As above, define  $\mathcal{F}_X$  as the subset of functions in  $\mathcal{F}$  that are constant in all components other than  $\Omega_X$ , for  $X \subset \{C, E, R\}$ . We say that  $\Omega_C$  **does not Koopman causally influence** component  $\Omega_E$  at time  $t$ , if  $K^t \mathcal{F}_E \subset \mathcal{F}_{E,R}$ . We denote this by  $\Omega_C \not\rightarrow_{\mathcal{K}}^t \Omega_E$ . Otherwise,  $\Omega_C$  **Koopman causally influences** component  $\Omega_E$  at time  $t$ , and we denote this by  $\Omega_C \rightarrow_{\mathcal{K}}^t \Omega_E$ . If for all  $t$  we have that  $\Omega_C$  does not Koopman causally influence component  $\Omega_E$ , we say that  $\Omega_C$  does not Koopman cause  $\Omega_E$ , and write  $\Omega_C \not\rightarrow_{\mathcal{K}} \Omega_E$ .

To make this definition explicit; the condition  $K^t \mathcal{F}_E \subset \mathcal{F}_{E,R}$  can be phrased in words as follows. Let  $f$  be a function that is constant on (at least) the component  $\Omega_C$ . If the Koopman-evolved function  $K^t f$  still does not depend on the component  $\Omega_C$ , i.e.  $K^t f \in \mathcal{F}_{E,R}$ , then there is no causality from component  $\Omega_C$  to  $\Omega_E$  as far as the Koopman operator can detect at time  $t$ . Thus,  $\Omega_C \not\rightarrow_{\mathcal{K}}^t \Omega_E$ . As a shorthand, the lack of a  $C$  subscript in  $\mathcal{F}_{E,R}$  means there is no dependence on component  $\Omega_C$ .

This definition is the equivalent of dynamical causality in the Koopman framework.

**Theorem III.2.** *Dynamical causal influence and Koopman causal influence are equivalent,*

$$\Omega_C \rightarrow_{\mathcal{K}}^t \Omega_E \iff \Omega_C \rightarrow \Omega_E$$

Correspondingly,

$$\Omega_C \not\rightarrow_{\mathcal{K}}^t \Omega_E \iff \Omega_C \not\rightarrow \Omega_E$$

See Appendix C 4 for the proof.

## IV. QUANTIFYING CAUSAL INFLUENCE FROM DATA WITH DMD KOOPMAN APPROXIMATIONS

The equivalence of dynamical causality and Koopman causality, given by Theorem III.2, opens new avenues to assess causality in nonlinear systems. The causal flow of observables that identify Koopman causality in Definition III.5 suggests a simple adaptation of the DMD algorithm to *quantify* causal relationships directly from data.

From Definition III.5, component  $\Omega_C$  has a causal effect on  $\Omega_E$  if the Koopman evolution of functions

in the component subspace  $\mathcal{F}_E$  induces a dependence on component  $\Omega_C$  in the resulting time-shifted functions. We can thus test how well  $\mathcal{K}^t \mathcal{F}_E$  can be represented in a basis of functions in the joint observable subspace  $\mathcal{F}_{E,C}$ . Said another way, we start with functions that depend only on component  $\Omega_E$  and then test how much dependence on component  $\Omega_C$  is added, or not, after evolving with a Koopman operator.

Intuitively, this is a way to quantify the unique causal contribution of  $\Omega_C$  on the evolution of component  $\Omega_E$ . If there are additional causal contributions from the remainder component  $\Omega_R$ , then  $\mathcal{K}^t \mathcal{F}_E$  cannot be completely represented in the basis  $\mathcal{F}_{E,C}$  since there are missing dependencies from  $\Omega_R$ . However, if  $\Omega_C$  encompasses the totality of causal influence on the evolution of  $\Omega_E$ , the  $\mathcal{K}^t \mathcal{F}_E$  can be fully represented in the joint basis  $\mathcal{F}_{E,C}$ . Note though, that if  $\Omega_E$  is an independent dynamical system with no additional causal influences, then  $\mathcal{K}^t \mathcal{F}_E$  will also be fully represented by the joint space  $\mathcal{F}_{E,C}$  because  $\mathcal{K}^t \mathcal{F}_E \subseteq \mathcal{F}_E$  and  $\mathcal{F}_E \subseteq \mathcal{F}_{E,C}$ . Therefore, we need to add a baseline comparison of how well  $\mathcal{K}^t \mathcal{F}_E$  can be represented by functions in the marginal state space  $\mathcal{F}_E$  that depend only on the ‘effect’ component  $\Omega_E$ .

### A. Data-Driven Causality Measures

With these insights, we now define a data-driven causality measure based on the DMD algorithm. This is done by fitting two different DMD models to evolve test functions in  $\mathcal{F}_E$ : a *joint model* that uses basis functions in  $\mathcal{F}_{E,C}$  and a *marginal model* that uses basis functions in  $\mathcal{F}_E$  only. By measuring the difference in these two models, we derive an empirical measure of nonlinear causality through the Koopman operator.

Our Koopman causality algorithm requires data from the chosen ‘cause’ and ‘effect’ components. The data must come as triples  $(\omega_E(n), \omega_E^t(n), \omega_C(n))$ , where  $\omega_E^t := P_E \Phi^t([\omega_E \ \omega_C \ \omega_R]^\top)$  is the time-shift of  $\omega_E$  and  $n$  is the time index of the data. We split the dataset into **train** and **test** sets.

Because we are testing how well functions  $\mathcal{F}_E$  can be represented in the joint space  $\mathcal{F}_{E,C}$  compared to the marginal space  $\mathcal{F}_E$  after Koopman evolution, the algorithm additionally requires separate dictionaries of basis functions for each of these spaces. For the input *test functions*  $f_E \in \mathcal{F}_E$ , we have found it best to use the identity observables  $f_E(\omega_E) = \omega_E$  in practice. Their efficacy is likely because the identity observables are generally not in a finite invariant subspace [33], and so adding additional basis functions tends to improve how well the model predicts these observables.

For both the joint and marginal models, we include the test functions (i.e. the identity observables) in the DMD function dictionary  $\Psi$ , along with the additional basis functions with which we want to express their time-shifts. We use random Fourier features for these additional basis functions—see Section II E.1. above. The marginal dictionary functions are given as

$$\psi_E(\omega_E) = \cos(\phi_E^\top \omega_E + b),$$

and the joint dictionary functions are

$$\psi_{E,C}(\omega_E, \omega_C) = \cos(\phi_{E,C}^\top [\omega_E \ \omega_C]^\top + b).$$

Using data matrices as defined above for dynamic mode decomposition, the **marginal model** is defined as

$$K_{\text{marg}}^t = \Omega_E^t \begin{bmatrix} \Omega_E \\ \Psi_E \end{bmatrix}^\dagger, \quad (14)$$

where  $\Psi_E$  is the data matrix formed by applying the marginal dictionary of random Fourier features  $\psi_E(\omega_E)$  to the training data matrix  $\Omega_E$ . The **joint model** is similarly defined as

$$K_{\text{joint}}^t = \Omega_E^t \begin{bmatrix} \Omega_E \\ \Psi_{E,C} \end{bmatrix}^\dagger, \quad (15)$$

with the data matrix  $\Psi_{E,C}$  formed from the joint dictionary of random Fourier features  $\psi_{E,C}(\omega_E, \omega_C)$  applied to the columns of  $\Omega_E$  and  $\Omega_C$ . The only difference between the two models is the additional dictionary functions of  $\Psi_E$  for the marginal model and  $\Psi_{E,C}$  for the joint model.

Note that we only care about the approximated Koopman evolution of the test functions in  $\mathcal{F}_E$ , hence the DMD models  $K_{\text{marg}}^t$  and  $K_{\text{joint}}^t$  are not square. For given values of  $\omega_E \in \Omega_E$  and  $\omega_C \in \Omega_C$ , the point-evaluation of the time-shifted test function  $[\mathcal{K}^t f_E](\omega_E \ \omega_C \ \omega_R)^\top := \omega_E^t$  is approximated by the marginal model as

$$\tilde{\omega}_E^t|_{\text{marg}} := K_{\text{marg}}^t \begin{bmatrix} \omega_E \\ \Psi_E(\omega_E) \end{bmatrix}, \quad (16)$$

and by the joint model as

$$\tilde{\omega}_E^t|_{\text{joint}} := K_{\text{joint}}^t \begin{bmatrix} \omega_E \\ \Psi_{E,C}(\omega_E, \omega_C) \end{bmatrix}. \quad (17)$$

For both cases, model error is evaluated over the set of **test** points  $\{\omega_E, \omega_E^t, \omega_C\}_{\text{test}}$

$$\text{model error} = \frac{1}{N_{\text{test}}} \sum_{\text{test}} \|\tilde{\omega}_E^t - \omega_E^t\|^2, \quad (18)$$

with the marginal model error given using  $\tilde{\omega}_E^t = \tilde{\omega}_E^t|_{\text{marg}}$  and the joint model error given using  $\tilde{\omega}_E^t = \tilde{\omega}_E^t|_{\text{joint}}$ .

We can now define our **data-driven measure of causality**, denoted  $\Omega_C \xrightarrow{K^t} \Omega_E$ , as

$$\Omega_C \xrightarrow{K^t} \Omega_E := \text{marginal error} - \text{joint error} . \quad (19)$$

**Remark 3.** Our causality measure is conceptually similar to Wiener-Granger causality [11, 12] in that we compare the predictive power of a marginal model to a joint model. In fact, if delay-coordinate embedding are used for the additional dictionary functions  $\Psi$  (known as delay DMD or Hankel DMD [34]) the marginal and joint model predictions in Eqns. (16) and (17) are functionally equivalent to those of Wiener-Granger causality—predictions are linear functions of past observables. Note though that the evaluation of model error in Wiener-Granger causality is typically different from Eqn. (18), typically comparing the variance of model residuals.

However, the implementation details and interpretation are different in our Koopman framework. Here, we are predicting the (always linear) evolution of system observables and comparing how well the evolution of test functions of component  $\Omega_E$  can be represented in a marginal basis of functions of component  $\Omega_E$  only versus how well they can be represented in a joint basis of functions of component  $\Omega_E$  and  $\Omega_C$ . While the causal measure  $\Omega_C \xrightarrow{K^t} \Omega_E$  is as simple to implement as Granger causality—both are linear regressions—the theory we have given provides a solid foundation to ground our measure. Moreover, because our measure is based on Koopman operators, it can be applied universally to all autonomous nonlinear dynamical systems.

**Example 4.** In Figure 2 we show  $\Omega_2 \xrightarrow{K^t} \Omega_1$  for many time shifts  $t$  of the coupled Rössler system with nonlinearity  $d = 5.7$  and coupling constants  $c_1 = 0.5$  and  $c_2 = 0.0$  (and so  $\Omega_2 \rightarrow \Omega_1$  and  $\Omega_1 \not\rightarrow \Omega_2$ ). The coupled Rössler system is continuous-time and we use an integration step  $\delta t = 0.01$  for data generation. Because the system is continuous-time, a small time shift  $t$ —given here as the number of integration steps—imparts a small causal dependence of  $\Omega_2$  onto  $\Omega_1$ . This is what we see in Figure 2 with a roughly linear dependence of  $\Omega_2 \xrightarrow{K^t} \Omega_1$  on  $t$  for  $t \leq 500$ . The causal dependence continues to grow until about  $t = 1000$  where it plateaus. Interestingly, around  $t = 1500$ , the causal dependence actually decreases momentarily, before increasing again back up to the plateau value by

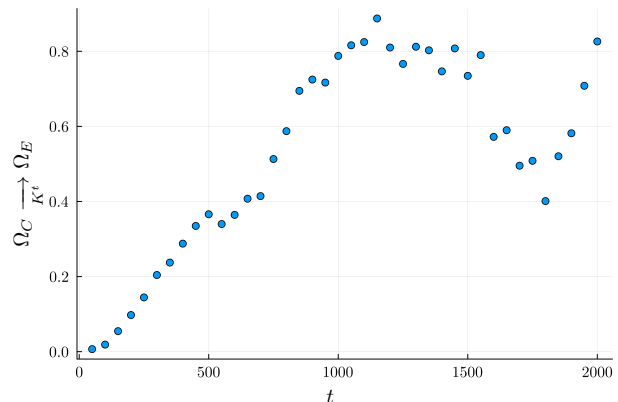


FIG. 2. Causal measure per time of coupled Rössler.

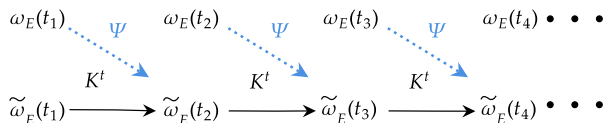


FIG. 3. Graphical depiction of a marginal conditional forecast for ‘effect’ component  $\Omega_E$ . Predicted values  $\tilde{\omega}_E(t_n)$  are fed back into the model, shown with solid black arrows, while values  $\omega_E(t_n)$  from the test data are plugged into the additional dictionary functions  $\Psi$ , as shown with dotted blue arrows.

$t = 2000$ . The Lyapunov time for this system is just under  $t = 1000$  time steps.

We emphasize again that while it is clear from the equations of motion that  $\Omega_2 \rightarrow \Omega_1$ , and it is intuitive that the causal effect should be low at short time scales, it is not at all obvious from inspecting the equations how the causal influence should behave at longer time scales. In Example 3, we emphasized the interplay between component coupling and nonlinearity in each components’ dynamics and how these combine in non-intuitive ways to produce causal effects. Nonlinear systems, like the Rössler oscillator, can experience intermittent bursting behaviors over longer time scales, which may contribute to the decreased causal influence we see between  $t = 1500$  and  $t = 2000$ .

## B. Causality Over Time with Conditional Forecasting

The causal measure in Eqn. (19) is the core data-driven tool to apply our Koopman theory of causality in practice. By definition, it determines causal influence *at the given time scale*  $t$ . One may be in-

terested more holistically in how the causal influence behaves over time. Because the causal measure in Eqn. (19) has to be computed at each time scale  $t$ , it can be costly to compute the temporal behavior of causal relations.

If the time shift  $t$  in the `training` set is small and the `test` set is a time series (sampled at the small shift  $t$ ), then we can assess causal relations over time much more efficiently using *conditional forecasting*. The term ‘forecasting’ is used because the algorithm sequentially feeds its output back into its input. However, we emphasize that these models *cannot* predict the evolution of the test functions for times outside the `test` set—the forecasts are ‘conditional’ because they require inputs from the `test` set. Of course, the goal here is to assess causality, and not to predict how the observables will evolve in the unseen future—standard DMD and its many variants are used for that.

**Conditional forecasting** utilizes the same form of marginal and joint models given in Eqns. (14) and (15), respectively, using the small time shift  $t$ . The models use dictionaries that consist of two pieces  $[\omega_E \ \Psi]^\top$  with  $\Psi = \Psi_E(\omega_E)$  for the marginal model and  $\Psi = \Psi_{E,C}(\omega_E, \omega_C)$  for the joint model. For both cases, we sequentially forecast the first piece (the identity observable test function), while the second piece,  $\Psi$ , is always evaluated using the corresponding values of  $\omega_E$  and  $\omega_C$  from the `test` set—see Figure 3. For the marginal case, we actually could use the predicted values of  $\omega_E$  to evaluate the dictionary functions  $\Psi_E(\omega_E)$ —this is just standard DMD. However, causal evaluation requires comparison of the marginal and joint models, so we use the same conditional forecasting procedure for both. We emphasize again that this ‘forecast’ only approximates the `test` time series  $\{\omega_E\}_{\text{test}}$ .

Given initial values  $(\omega_E(t_0), \omega_C(t_0))$  from the `test` data, the conditional forecast proceeds as follows. The first prediction is made using the initial `test` values as

$$\tilde{\omega}_E(t_1)|_{\text{marg}} = K_{\text{marg}}^t \begin{bmatrix} \omega_E(t_0) \\ \Psi_E(\omega_E(t_0)) \end{bmatrix},$$

for the marginal model and

$$\tilde{\omega}_E(t_1)|_{\text{joint}} = K_{\text{joint}}^t \begin{bmatrix} \omega_E(t_0) \\ \Psi_{E,C}(\omega_E(t_0), \omega_C(t_0)) \end{bmatrix},$$

for the joint model. The next time step is predicted as

$$\tilde{\omega}_E(t_2)|_{\text{marg}} = K_{\text{marg}}^t \begin{bmatrix} \tilde{\omega}_E(t_1) \\ \Psi_E(\omega_E(t_1)) \end{bmatrix},$$

for the marginal model and

$$\tilde{\omega}_E(t_2)|_{\text{joint}} = K_{\text{joint}}^t \begin{bmatrix} \tilde{\omega}_E(t_1) \\ \Psi_{E,C}(\omega_E(t_1), \omega_C(t_1)) \end{bmatrix},$$

for the joint model. Note that the previously predicted value  $\tilde{\omega}_E(t_1)$  is fed back in for the identity piece of the dictionary for both models. This procedure continues in the same way for the duration of the `test` time series, with predicted values being fed back into the first piece of the model dictionary and the second additional dictionary elements always evaluated with values directly from the test data.

The marginal and joint model errors can be evaluated, similar to the counterfactual causality measure in Eqn.(13), by taking the mean-square error between the `test` series and conditional forecasts. One benefit of the conditional forecasting approach is that it provides a visualization of how well the marginal and joint models perform in predicting the `test` time series, as we now demonstrate with the Rössler system.

**Example 5.** Figure 4 shows conditional forecasts for the  $\Omega_2 \rightarrow \Omega_1$  coupled Rössler system. The left column shows forecasts for  $\Omega_2 \rightarrow \Omega_1$  and the right for  $\Omega_1 \rightarrow \Omega_2$ .

In the left column, we see non-zero prediction error from the marginal model, even though values from the `test` data are used at each step to evaluate  $\Psi_1(\omega_1)$ . The error occurs because the marginal model has no information from component  $\Omega_2$  that causally influences  $\Omega_1$ . When this information from  $\Omega_2$  is incorporated in the joint model, it is able to predict  $\Omega_1$  over at least 2000 time steps (with integration step size  $\delta = 0.01$ ) with very little error. Because the remainder component here is empty and  $\Omega = \Omega_1 \times \Omega_2$ , the ‘cause’ component  $\Omega_C = \Omega_2$  captures all causal influences on the ‘effect’  $\Omega_E = \Omega_1$ . As also observed in Figure 2, the marginal model is able to predict reasonably well for several hundred time steps before significant error occurs. For continuous-time systems, causal influence takes some time to propagate.

The right column switches roles of the components, with  $\Omega_C = \Omega_1$  and  $\Omega_E = \Omega_2$  to test whether component  $\Omega_1$  causally influences  $\Omega_2$ , which we know it does not since  $c_2 = 0$ . As expected then, we see essentially no difference in the predictions of the marginal and joint models. Because there are no external causal influences on  $\Omega_2$ , the marginal function space  $\mathcal{F}_2$  of component  $\Omega_2$  is Koopman-invariant  $\mathcal{K}^t \mathcal{F}_2 \subseteq \mathcal{F}_2$ . The evolution of test functions are thus well-expressed in the marginal basis  $\mathcal{F}_2$  (which also requires that the RFF basis functions cover the space reasonably well).

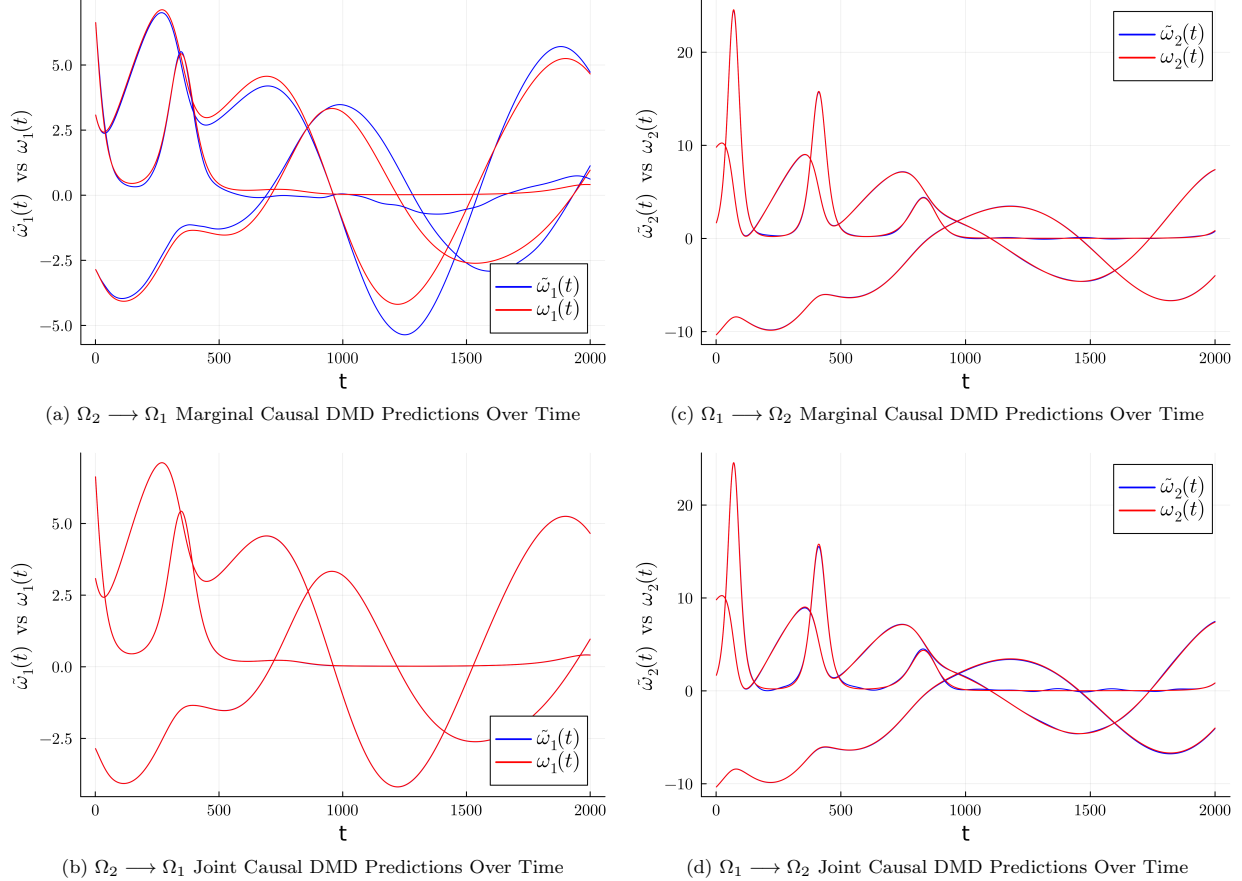


FIG. 4. Conditional forecasts for  $\Omega_2 \rightarrow \Omega_1$ ,  $\Omega_1 \not\rightarrow \Omega_2$  coupled Rössler system.

## V. APPLICATION TO SPATIOTEMPORAL SYSTEMS

Up to this point we have used the coupled Rössler system as the guiding example to demonstrate our theory and numerical causal measure. We now explore more complex systems to highlight the utility of our Koopman-based causal measure. In particular, we use the Lorenz 96 system as an idealized spatiotemporal system to show how our measure can discover structural properties of a system directly from data. In particular, asymmetrical coupling between oscillators in the Lorenz 96 model leads to an asymmetrical causal flow over space through time that our causal measure can identify. We will see that our Koopman causality measure identifies a causal wave that propagates in the same direction and at roughly the same speed that information propagates in the system, as identified through perturbation propagation.

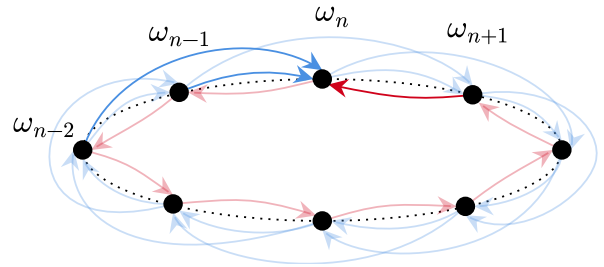


FIG. 5. Asymmetry in the spatial coupling between oscillators of the Lorenz 96 model.

### A. The Lorenz 96 System

The Lorenz 96 system is an idealized model of the dynamics of a scalar quantity in the atmosphere [35]. It consists of  $N$  sites on a ring, which are viewed as  $N$  equally spaced locations on a single line of latitude on the Earth. Each degree of freedom  $\omega_n$  on an

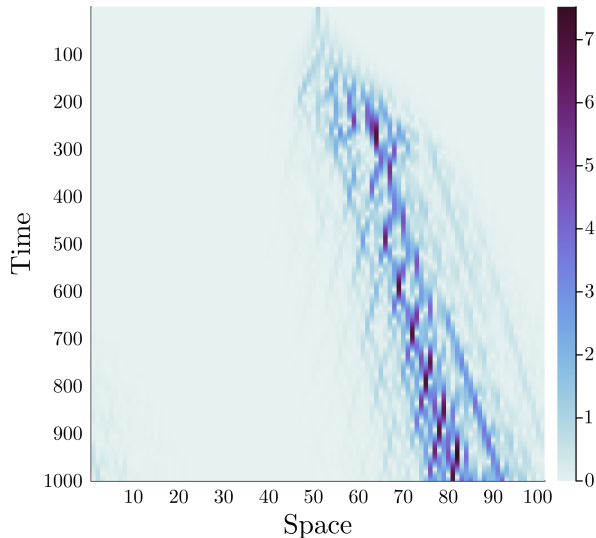


FIG. 6. Perturbation propagation in the Lorenz 96 model. The spacetime diagram depicts the (absolute value) difference between two orbits of the Lorenz 96 model that have identical initial conditions except for a perturbation in the central oscillator. This experiment indicates that information propagates in the system as a traveling wave in the clockwise direction.

individual site  $n$  evolve according to

$$\dot{\omega}_n = (\omega_{n+1} - \omega_{n-2})\omega_{n-1} - \omega_n + F. \quad (20)$$

We will refer to the  $\omega_n$  simply as ‘oscillators’. The last term  $F \geq 0$  is the *forcing*, as it is the rate at which the scalar quantity is added uniformly into the system. It is the only free parameter of this formulation of the model and controls how chaotic the system orbits are. The middle term,  $-\omega_n$ , is the *dissipation* term that dictates the rate of loss of the scalar quantity over time.

Finally, the most important term for our purposes here is the first,  $(\omega_{n+1} - \omega_{n-2})\omega_{n-1}$ . Because of the asymmetry in spatial coupling, this is the *advection* term. The dynamics of the oscillator  $\omega_n$  at site  $n$  depends only on the nearest neighbor in the clockwise direction  $\omega_{n+1}$ , but it depends on both the nearest  $\omega_{n-1}$  and next-nearest  $\omega_{n-2}$  neighbors in the counterclockwise direction; see Figure 5. The imbalance in spatial coupling leads to a clockwise transport of the quantity in the system over time.

For our experiments we use  $N = 101$  oscillators and a moderate forcing value of  $F = 4.0$ .

Due to the simplicity of the model, intuition about material transport translates closely to a ‘causal flow’ in the Lorenz 96 system. For now, consider each individual oscillator as its own component, i.e.

$\Omega_n = \{\omega_n\}$ . As time increases, the component flow maps  $P_n \Phi^t$  will depend on more components in the counterclockwise direction than the clockwise due to the asymmetric coupling discussed above. Thus, there is a dominant clockwise causal flow in the system similar to the clockwise material transport.

### 1. Perturbation Propagation and Information Flow

Before applying our Koopman causality measure, we first identify a baseline for comparison. We perform a perturbation propagation experiment in which we evolve a Lorenz 96 model from random initial conditions and then evolve a second model with the same initial conditions except for a perturbation applied to the oscillator at the middle site  $n = 51$ . As discussed by, e.g., Ref. [36], perturbation spreading indicates how *information* propagates through space over time in the system. A more recent example is the popular ‘slinky drop’ experiment [37]. A long slinky is held vertical, from the top, and then dropped. Slow motion video reveals that the bottom of the slinky does not move until the rest of the slinky reaches it. A common explanation is that the bottom of the slinky ‘does not know’ that the top has been released until that information reaches the bottom, and information propagates at the (relatively slow) longitudinal wave speed of the slinky.

A spacetime diagram of perturbation spreading in the Lorenz 96 model is shown in Figure 6, with spatial sites on the horizontal axis and time on the vertical increasing from top to bottom. From this, we see that information travels almost exclusively in the clockwise direction (increasing  $n$ ), at a finite speed. Similar to the slinky drop, the other oscillators do not instantly ‘know’ that the central oscillator has been perturbed. Information about the central oscillator perturbation travels to distant oscillators at a finite rate, due to the locality of interactions between the oscillators. It is notable that the local coupling occurs in *both* directions, as depicted in Figure 5, but the spatial asymmetry and cyclic feedback of the local coupling conspire to give a net flow of information in the clockwise direction, as seen in Figure 6.

### 2. Koopman Analysis and Causal Flow

The information flow analysis just described is achieved through perturbing the system. Similar to counterfactual experiments, this requires exact control over the system to very high precision, which is not realistic in practice. We now apply our Koopman causal measure to the Lorenz 96 system, and

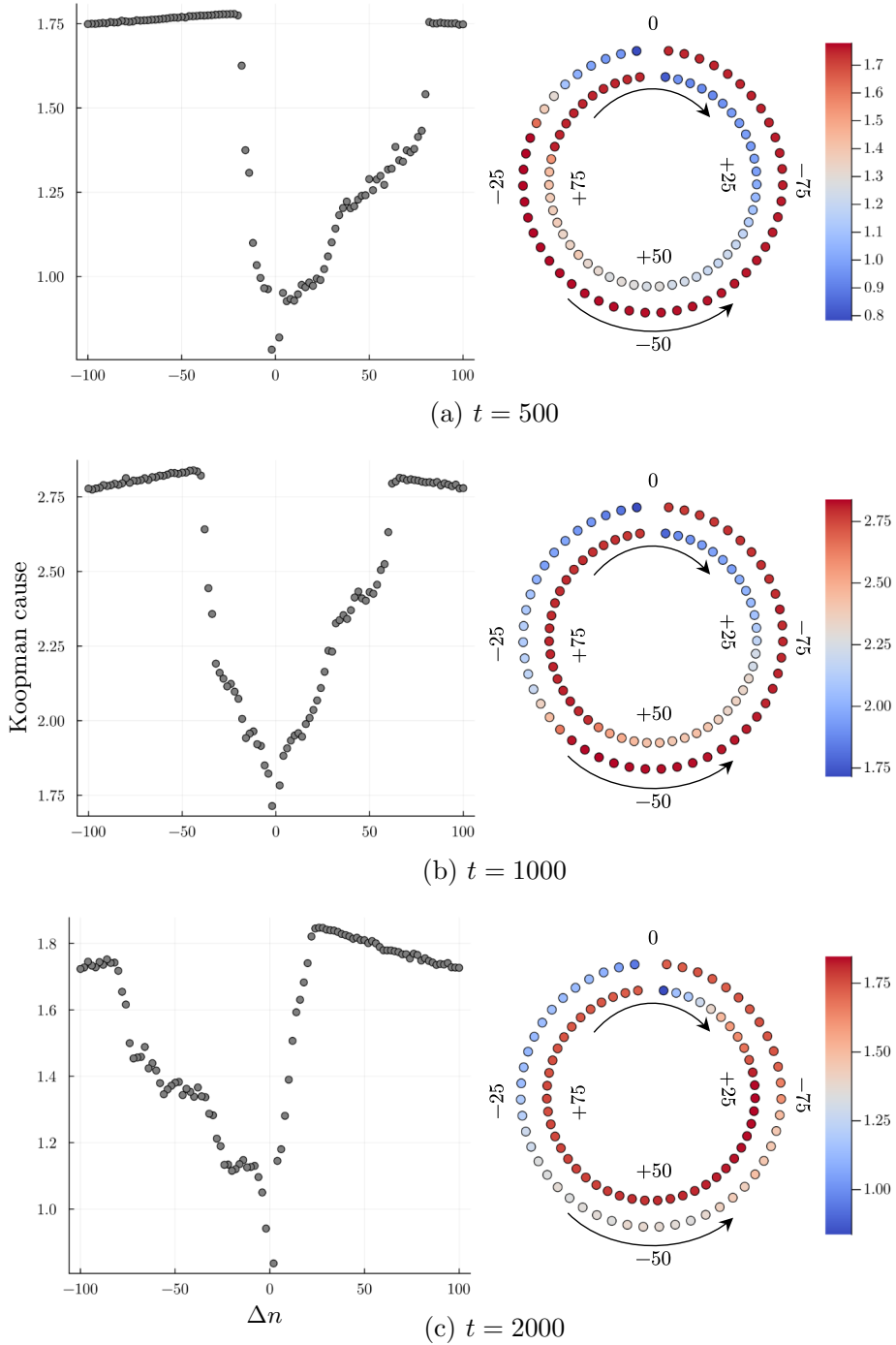


FIG. 7. Cumulative causal effects in the Lorenz 96 model.

again emphasize it is purely observational and does not require interventions (e.g., perturbations). Information flow is often assumed to be synonymous with causal flow such that causality is identified through measures of information flow. For example,

transfer entropy, a measure of information flow, is a nonlinear generalization of Wiener-Granger causality. Through comparison with the perturbation propagation in Figure 6, our Koopman causality measure reveals that there is indeed a close corre-



spondence between causal flow and information flow in the Lorenz 96 system.

Consider a ‘target site’  $n^*$ —it does not matter which specific site we choose since the Lorenz 96 system, as a whole, is rotationally symmetric. We want to identify the causal effects of other oscillators on the target oscillator  $\omega_{n^*}$ , so we designate the ‘effect’ component  $\Omega_E$  as the singleton  $\{\omega_{n^*}\}$ . Because causal flows must follow the spatial ring structure of the Lorenz 96 model, oscillators on the opposite side of the ring do not “directly” influence the target oscillator through their local interactions. Their causal influence must propagate over space to reach the target oscillator indirectly through the oscillators between them. We therefore examine the *cumulative* causal effects of increasingly-large sets of neighbors on the target oscillator. For the ‘cause’ component, we take all neighbors to and including the *neighbor number*  $\Delta n$ , with the direction of neighbors taken given by the sign of the neighbor number. For example, with  $\Delta n = 2$  we take the clockwise nearest and next-nearest neighbors for the ‘cause’ component  $\Omega_C$ . For  $\Delta n = -4$  we have  $\Omega_C = \{\omega_{n^*-1}, \omega_{n^*-2}, \omega_{n^*-3}, \omega_{n^*-4}\}$ , etc.

Figure 7 shows results of  $\Omega_C \xrightarrow{K^t} \Omega_E$  for the cumulative  $\Omega_C$  components at three different time shifts,  $t = \{500, 1000, 2000\}$ . For each time shift (each row in the Figure), there are two different plots that display the same results. The scatter plots in the left column show the causal effect values  $\Omega_C \xrightarrow{K^t} \Omega_E$  on the vertical axis, and the horizontal axis is the neighbor number  $\Delta n$  that gives cumulative  $\Omega_C$  component just defined. Thus, moving left from the center of each plot shows the cumulative causal effect of increasingly many counterclockwise neighbors out to  $\Delta n = -100$ , for which  $\Omega_C$  contains all other oscillators aside from the target. Similarly, moving right from center shows the cumulative causal effect of increasingly many clockwise neighbors out to  $\Delta n = 100$ , for which  $\Omega_C$  again contains all other oscillators aside from the target.

The circle plots in the right column also show  $\Omega_C \xrightarrow{K^t} \Omega_E$  for the same values of  $\Delta n$ . These are spatial embeddings of the scatter plots, with the value of the causal effect given by the color on each plot marker. The outer ring is equivalent to the left side of the scatter plots with negative  $\Delta n$ —the counterclockwise neighbors. The inside ring is the clockwise neighbors with positive  $\Delta n$ , and is equivalent to the right half of the scatter plots.

Collectively in Figure 7 we see a plateau in the value of the cumulative causal effect  $\Omega_C \xrightarrow{K^t} \Omega_E$  that travels counterclockwise over time, which corresponds to a propagating front of *causal flow* that travels clockwise over time. This is easiest to

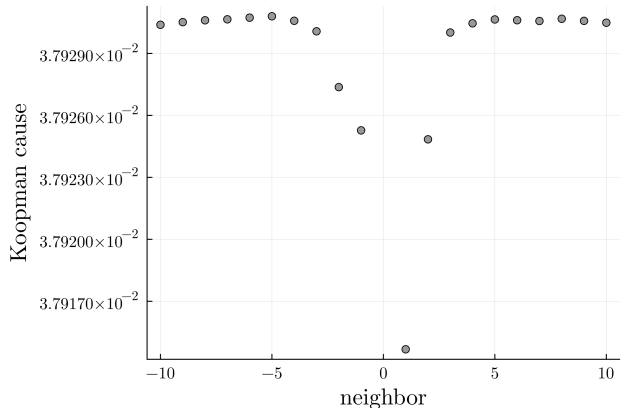


FIG. 8. Cumulative causal effects approximating the differential time scale.

see from inspecting the cumulative causal effect of the counterclockwise neighbors—those with negative neighbor numbers. Again, we are measuring the cumulative effect of neighbors on the target oscillator, and counterclockwise neighbors to the target is in the clockwise direction. So the cumulative effect of counterclockwise neighbors is measuring in the same direction that the front is traveling.

Starting at the shortest time step  $t = 500$ , the causal flow front has the least amount of time to travel and so travels the shortest distance. Therefore  $t = 500$  has the fewest counterclockwise neighbors that can effect the target through the propagating front of causal flow. Any additional counterclockwise neighbors added cannot contribute via the front of causal flow, hence the plateau. As we increase to  $t = 1000$  and  $t = 2000$  we see a smaller and smaller plateau because the front has more time to travel further, and hence more counterclockwise neighbors can effect the target oscillator via the front. This is exactly what we see in Figure 7. Significantly, the spatial location of the front at  $t = 500$  (around  $\Delta n = -20$ ) and  $t = 1000$  (around  $\Delta n = -30$ ) agree with perturbation front locations in Figure 6.

The cumulative causal effect of clockwise neighbors measures causation that does not follow the clockwise causal flow front, at least for small enough neighbor numbers. Because the Lorenz 96 model is on a ring, if you add enough clockwise neighbors you eventually come to the causal flow front from behind, where we again see a plateau in the values of our causal measure  $\Omega_C \xrightarrow{K^t} \Omega_E$ . The plateau in the clockwise direction occurs at roughly the same location on the ring as in the counterclockwise direction, as best seen from the circle plots in the right column of Figure 7.

To summarize, Figure 7 shows that our Koopman

causality measure identifies the dominant clockwise causal flow in the Lorenz 96 system. And, the causal flow we identify travels in the same direction and at roughly the same speed as the flow of information identified by perturbation propagation in Figure 6.

### 3. Instantaneous Causal Effects and Direct Influence

The above analysis implicitly assumed knowledge of the spatial ring structure of the Lorenz 96 model. This structure arises from the coupling between oscillators in the advection term of the equations of motion (20). Recall that for continuous-time dynamical systems, the differential equations of motion are the time derivatives of the flow maps. And, since causality in dynamical systems arises from the flow maps, the differential equations of motion represent *instantaneous causal effects*. There is often an emphasis in causality literature on ‘direct’ vs ‘indirect’ causal influence [2, 38]. From our rigorous formulation of dynamical system causality, it is clear that the use of ‘direct’ causation in dynamical systems really means ‘instantaneous’ causation. ‘Indirect’ causation occurs at later times when the flow maps pickup additional dependencies not present in the differential equations of motion.

To investigate instantaneous causation using our Koopman causality measure, we perform the same cumulative causal analysis as above at a very small time scale—we use an equivalent of  $t = 0.1$  (i.e., one time step using an integration time of  $\delta = 0.001$  compared to  $\delta = 0.01$  used in Figure 7). The results are shown in Figure 8. We can see that there is an asymmetry between clockwise and counterclockwise and the causal effect plateaus quickly in both directions. However, it is not clear from this analysis that the instantaneous causation includes one clockwise neighbor and two counterclockwise neighbors.

Because instantaneous causal effects arise from the differential equations of motion, they can be identified using equation discovery methods [39, 40]. Moreover, the time derivative of the Koopman semigroup is the Koopman generator—the Koopman equivalent of the equations of motion. It has been shown that equation discovery algorithms are special cases of approximation methods for the Koopman generator [41]. Thus, in principle, our Koopman method is capable of identifying direct causal effects in some cases. The results in Figure 8 are essentially equivalent to approximating the Koopman generator from finite differences, using marginal and joint dictionaries. We thus find that this straightforward method is not sufficient for approximating the Koopman generator of this Lorenz 96 model, even using very small differences. Other methods, such

as automatic differentiation, could potentially find the correct instantaneous causal relations.

To close, remember that in many cases of interest we *do* know the governing equations and thus the topology of direct causal relations (though not necessarily their magnitudes). What is not clear, for many complex systems, is how these causal relations unfold as time evolves. We again emphasize that the flow maps for these systems are complicated and do not have closed-form analytic solutions. The strength of our data-driven Koopman causality method is its ability to discover causal relations at non-instantaneous time scales.

## VI. DISCUSSION

The existing tools for causality in dynamical systems largely fall into two categories based on either i) information flows, or ii) delay coordinate embeddings. Having introduced our Koopman theory of causality, we now overview how it relates to these other methods. Conceptually, it is most similar to information flows. In fact, information flows in deterministic dynamical systems can be formulated in terms of Perron-Frobenius operators [8], which are dual to Koopman operators [21]—they evolve probability distributions over systems states, rather than observables of the system states.

Note that information flow is a more general concept that extends beyond causal discovery, and so measures to quantify information flow, such as transfer entropy [18], are not necessarily designed to be measures of causality. Additional axioms are typically posited to identify causal flows through information flows, notably *asymmetry*—the causal flow from  $\Omega_2$  to  $\Omega_1$  is not necessarily the same as from  $\Omega_1$  to  $\Omega_2$ —and *nil causality*—if  $\Omega_2 \not\rightarrow \Omega_1$  then the causal flow from  $\Omega_2$  to  $\Omega_1$  should be zero. From Figure 3 we can see that our Koopman causality measure satisfies these axioms. Additional work is necessary to more rigorously connect our Koopman causality framework to information flows through the duality of Koopman and Perron-Frobenius operators.

The other category of causal methods for dynamical systems are those based on delay coordinate embeddings, most notably convergent cross mapping [13]. Whereas information flows are more of a ‘top down’ approach to causality, delay embedding methods are ‘bottom up’, with its definition of causality rigorously based on the ability of past histories of some degrees of freedom to encode the effects of other degrees of freedom in the system [17]. Interestingly, while our Koopman theory is similarly ‘bottom up’, starting from the rigorous Defi-

dition III.3 of dynamical system causality, it does *not* utilize delay embeddings. In order to quantify the unique causal influence of one component on another, particularly in the presence of additional unobserved components (the ‘remainder’), we do not want to encode the effects of other degrees of freedom. Our approach provides a tractable means to do this through the global linearization of Koopman operators.

Finally, we note that the practical application of our data-driven causality measure is limited by the quality of the DMD approximation to the Koopman operators used in the marginal and joint models. If the DMD models give very poor approximations to the evolution of the identity observable (or other test functions in  $\mathcal{F}_E$ , more generally), then the comparison of marginal and joint model errors is not necessarily reflective of causal relations in the system. In particular, the class of DMD models used in this work do not reliably give good approximations for chaotic systems.

That said, our framework allows for the use of more sophisticated Koopman approximations to give more robust data-driven measures of causality. Alternatively, it may be possible to use our Koopman theory to define a measure of causality based on defects between component subspaces. If  $\Omega_C \not\rightarrow \Omega_E$  then  $\mathcal{K}^t \mathcal{F}_E \subseteq \mathcal{F}_{E,R}$ , and so a possible route to measure causal effects would be to identify the defect between  $\mathcal{K}^t \mathcal{F}_E$  and  $\mathcal{F}_{E,R}$ . The ‘‘principal angle’’ between these space [42] is a promising approach to quantify this defect from data.

## VII. CONCLUSION

We have introduced a new theory of causality in nonlinear dynamical systems using Koopman operators. Our theory is based on a rigorous definition of causal mechanism in dynamical systems using flow maps, analogous to the standard definition of causal mechanism in structural causal models. We defined

causality in the Koopman framework as flows between function subspaces, and proved that this is equivalent to the definition of causal mechanism using flow maps. Our Koopman theory of causality lends itself to a straightforward data-driven measure of causality based on the dynamic mode decomposition algorithm. After giving some basic demonstrations on the coupled Rössler system, we showed that our data-driven causality measure can identify causal flow in the Lorenz 96 model associated with advective transport, in agreement with information flow identified in a perturbation propagation experiment.

In addition to providing a rigorous foundation of causal mechanisms for dynamical systems, our data-driven Koopman causality measure provides new capabilities not found in most causality algorithms for dynamical systems. The definition of causal mechanism in terms of flow maps clarifies the importance of time scale, and our Koopman method identifies relations at a chosen time scale. It also naturally incorporates multivariate (or polyadic) causal relationships [10] through the flexible definition of components. Because DMD can scale to high-dimensional systems, our method can evaluate causal relations between high-dimensional components. Time series causality methods, by contrast, first require a dimensionality reduction step, and so can only evaluate causal relationships between the reduced components.

## ACKNOWLEDGMENTS

This work was supported by the U.S. Department of Energy (DOE), Office of Science, Office of Biological and Environmental Research, Regional and Global Model Analysis program area as part of the HiLAT-RASM project. The Pacific Northwest National Laboratory (PNNL) is operated for DOE by Battelle Memorial Institute under contract DE-AC05-76RLO1830.

- 
- [1] A. Rupe and J. P. Crutchfield, *Physics Reports* **1071**, 1 (2024).
  - [2] J. Runge *et al.*, *Nature communications* **10**, 1 (2019).
  - [3] G. Camps-Valls, A. Gerhardus, U. Ninad, G. Varando, G. Martius, E. Balaguer-Ballester, R. Vinuesa, E. Diaz, L. Zanna, and J. Runge, *Physics Reports* **1044**, 1 (2023).
  - [4] J. Pearl, *Causality* (Cambridge university press, 2009).
  - [5] M. Ghil and V. Lucarini, *Reviews of Modern Physics* **92**, 035002 (2020).
  - [6] G. Roe, *Annual Review of Earth and Planetary Sciences* **37**, 93 (2009).
  - [7] T. M. Merlis, *Geophysical Research Letters* **41**, 7291 (2014).
  - [8] X. S. Liang and R. Kleeman, *Physical review letters* **95**, 244101 (2005).
  - [9] N. Ay and D. Polani, *Advances in complex systems* **11**, 17 (2008).

- [10] R. G. James, N. Barnett, and J. P. Crutchfield, *Physical review letters* **116**, 238701 (2016).
- [11] W. N., *Modern Mathematics for Engineers*; Beckenbach, E.F., Ed.; McGraw-Hill: New York, NY, USA (1956).
- [12] C. W. Granger, *Econometrica: journal of the Econometric Society*, 424 (1969).
- [13] G. Sugihara, R. May, H. Ye, C.-h. Hsieh, E. Deyle, M. Fogarty, and S. Munch, *Science* **338**, 496 (2012).
- [14] D. Harnack, E. Laminski, M. Schünemann, and K. R. Pawelzik, *Phys. Rev. Lett.* **119**, 098301 (2017).
- [15] A. A. Tsonis, E. R. Deyle, H. Ye, and G. Sugihara, *Advances in nonlinear geosciences*, 587 (2018).
- [16] N. H. Packard, J. P. Crutchfield, J. D. Farmer, and R. S. Shaw, *Phys. Rev. Lett.* **45**, 712 (1980).
- [17] F. Takens, in *Symposium on Dynamical Systems and Turbulence*, Vol. 898, edited by D. A. Rand and L. S. Young (Springer-Verlag, Berlin, 1981) p. 366.
- [18] T. Schreiber, *Physical review letters* **85**, 461 (2000).
- [19] S. L. Brunton, M. Budišić, E. Kaiser, and J. N. Kutz, *SIAM Review* **64**, 229 (2022).
- [20] E. Bareinboim, J. D. Correa, D. Ibeling, and T. Icard, in *Probabilistic and causal inference: the works of Judea Pearl* (2022) pp. 507–556.
- [21] A. Lasota and M. C. Mackey, *Chaos, fractals, and noise: stochastic aspects of dynamics*, Vol. 97 (Springer Science, 1994).
- [22] J. Milnor and W. Thurston, *Springer Lecture Notes* **1342**, 465 (1988).
- [23] P. Collet and J.-P. Eckmann, *Maps of the Unit Interval as Dynamical Systems* (Birkhauser, Berlin, 1980).
- [24] V. I. Paulsen and M. Raghupathi, *An introduction to the theory of reproducing kernel Hilbert spaces*, Vol. 152 (Cambridge university press, 2016).
- [25] E. Gonzalez, M. Abudia, M. Jury, R. Kamalapurkar, and J. A. Rosenfeld, *arXiv preprint arXiv:2106.00106* (2021).
- [26] J. D. Meiss, *Differential dynamical systems* (SIAM, 2007).
- [27] B. O. Koopman, *Proc. Natl. Acad. Sci. USA* **17**, 315 (1931).
- [28] M. O. Williams, I. G. Kevrekidis, and C. W. Rowley, *Journal of Nonlinear Science* **25**, 1307 (2015).
- [29] S. Klus, P. Koltai, and C. Schütte, *Journal of Computational Dynamics* **3**, 51 (2016).
- [30] M. Korda and I. Mezić, *Journal of Nonlinear Science* **28**, 687 (2018).
- [31] A. Rahimi and B. Recht, *Advances in neural information processing systems* **20** (2007).
- [32] M. A. Hernán and S. L. Taubman, *International journal of obesity* **32**, S8 (2008).
- [33] S. L. Brunton, B. W. Brunton, J. L. Proctor, and J. N. Kutz, *PloS one* **11**, e0150171 (2016).
- [34] H. Arbabi and I. Mezić, *SIAM Journal on Applied Dynamical Systems* **16**, 2096 (2017).
- [35] J. Kerin and H. Engler, *Discrete and Continuous Dynamical Systems - B* **27**, 769 (2022).
- [36] N. H. Packard and S. Wolfram, *Journal of Statistical physics* **38**, 901 (1985).
- [37] D. Muller, Slinky drop answer, Veritasium, <https://www.youtube.com/watch?v=eCMMmEEy000> (Accessed: 2024-10-02).
- [38] J. Sun, D. Taylor, and E. M. Bollt, *SIAM Journal on Applied Dynamical Systems* **14**, 73 (2015).
- [39] J. P. Crutchfield and B. S. McNamara, *Complex Systems* **1**, 417 (1987).
- [40] S. L. Brunton, J. L. Proctor, and J. N. Kutz, *Proceedings of the national academy of sciences* **113**, 3932 (2016).
- [41] S. Klus, F. Nüske, S. Peitz, J.-H. Niemann, C. Clementi, and C. Schütte, *Physica D: Nonlinear Phenomena* **406**, 132416 (2020).
- [42] F. Deutsch, in *Approximation theory, wavelets and applications* (Springer, 1995) pp. 107–130.
- [43] G. Gundersen, *Random Fourier features*, <https://gregorygundersen.com/blog/2019/12/23/random-fourier-features/> (2019), accessed: 2010-09-30.
- [44] W. Rudin, *Fourier analysis on groups* (Wiley-Interscience, 1994).

## Appendix A: Random Fourier Features and RKHS

It is instructive to briefly go through the relation between random Fourier features and kernels. In particular, tensor products of Gaussian-distributed random Fourier features approximate tensor product Gaussian kernels. We largely follow the exposition in Reference [43].

Let  $\mathcal{V}$  be a Hilbert space. A function  $\varphi : \Omega \rightarrow \mathcal{V}$  is called a *feature map*. A feature map naturally defines a kernel, and hence a RKHS via

$$K(\omega, \omega') = \langle \varphi(\omega), \varphi(\omega') \rangle_{\mathcal{V}} ,$$

Given a kernel function  $K$  over  $\Omega$ , there may be many feature maps which represent the kernel:  $K(\omega, \omega') = \langle \varphi(\omega), \varphi(\omega') \rangle_{\mathcal{V}}$ . The map  $\varphi(\omega) = k_{\omega}$  is one example, but in general there will be many more.

Random Fourier features are random functions  $\Psi : \Omega \rightarrow \mathbb{R}^M$  that approximate the kernel as

$$K(\omega, \omega') = \langle \varphi(\omega), \varphi(\omega') \rangle_{\mathcal{V}} \approx \Psi(\omega)^{\top} \Psi(\omega') .$$

From Bochner’s theorem [44], the Fourier transform of a non-negative measure gives a continuous, positive definite, and shift-invariant kernel  $K(\omega, \omega') = K(\omega - \omega')$ ,

$$K(\omega - \omega') = \int p(\phi) e^{i\phi^{\top}(\omega - \omega')} d\phi .$$

Let  $\psi(\omega) = e^{i\phi^{\top}\omega}$  and normalize the non-negative measure  $p(\phi)$  so that it is a probability measure. The Fourier transform becomes an expectation over

$\phi$  and we take  $M$  IID samples  $\{\phi_j\}_{j=1}^M$  for a Monte Carlo approximation,

$$\begin{aligned} \mathsf{K}(\omega - \omega') &= \int p(\phi) e^{i\phi^\top(\omega - \omega')} d\phi \\ &= \mathbb{E}_\phi [e^{i\phi^\top(\omega - \omega')}] \\ &\approx \frac{1}{R} \sum_{j=1}^M e^{i\phi_j^\top(\omega - \omega')} \\ &= \begin{bmatrix} \frac{1}{\sqrt{M}} e^{i\phi_1^\top \omega} \\ \frac{1}{\sqrt{M}} e^{i\phi_2^\top \omega} \\ \vdots \\ \frac{1}{\sqrt{M}} e^{i\phi_M^\top \omega} \end{bmatrix}^\top \begin{bmatrix} \frac{1}{\sqrt{M}} e^{-i\phi_1^\top \omega'} \\ \frac{1}{\sqrt{M}} e^{-i\phi_2^\top \omega'} \\ \vdots \\ \frac{1}{\sqrt{M}} e^{-i\phi_M^\top \omega'} \end{bmatrix} \\ &:= \Psi(\omega) \Psi(\omega')^* . \end{aligned}$$

Now consider a system with  $L$  components,  $\omega = [\omega_1 \ \omega_2 \ \dots \ \omega_L]^\top$ . Let  $\psi_i(\omega_i) := e^{i\phi_i^\top \omega_i}$  for  $i \in \{1, \dots, L\}$ . Taking the tensor product of the component random Fourier feature functions, we get

$$\begin{aligned} [\psi_1 \otimes \psi_2 \otimes \dots \otimes \psi_L](\omega) &= \prod_{i=1}^L \psi_i(\omega_i) \\ &= e^{i\phi_1^\top \omega_1} e^{i\phi_2^\top \omega_2} \dots e^{i\phi_L^\top \omega_L} \\ &= e^{i(\phi_1^\top \omega_1 + \phi_2^\top \omega_2 + \dots + \phi_L^\top \omega_L)} \\ &= e^{i\phi^\top \omega} \\ &= \psi(\omega) , \end{aligned}$$

where  $\phi = [\phi_1 \ \phi_2 \ \dots \ \phi_L]^\top$ . Therefore, the tensor product of component random Fourier features is also a random Fourier feature.

We will use random Fourier features as dictionary basis functions. From the discussion above, this dictionary approximates the kernel associated to a given shift invariant kernel which arises from a feature map. This will allow us to create random projections of Koopman operators into a given RKHS function space  $\mathcal{F}$ . This applies for the full space  $\mathcal{F}$  as well as component spaces  $\mathcal{F}_i$ .

Since we use Koopman approximations in this work to evolve real-valued functions, we utilize real-valued random Fourier feature dictionaries. Together with some trigonometric manipulations and  $b \sim \text{Uniform}(0, 2\pi)$ , this gives our random Fourier feature dictionary in Eqn. (10),

$$\Psi_{\text{RFF}}(\omega) = [\psi_1(\omega) \ \dots \ \psi_M(\omega)]^\top ,$$

with  $\psi_j(\omega) = \cos(\phi_j^\top \omega + b)$ .

We note that Gaussian radial basis functions (RBFs) also have the above property that they can be used to define both the full RKHS space  $\mathcal{F}$  as well

as the component spaces  $\mathcal{F}_i$ . Each RBF dictionary function is given by a different choice of center  $\omega'$ , which can be chosen, e.g., uniformly or randomly. In practice, we have found it easier to do parameter optimizations with Gaussian random Fourier features than with Gaussian RBFs. Both are valid dictionary choices for the causal discovery algorithms we introduce below, and we have found similar performance when parameters are optimized manually.

## Appendix B: Feedback Phenomenology of Coupled Rössler System

Here we consider the fully-coupled case of the coupled Rössler system with both  $c_1 \neq 0$  and  $c_2 \neq 0$ . There are feedbacks in this system such that each component has a causal influence on itself at later times, mediated through the other component. That is, the feedback of  $\Omega_1$  on itself is the combined causal effect of  $\Omega_1 \rightarrow \Omega_2$  and then  $\Omega_2 \rightarrow \Omega_1$ .

To get some notion of the strength of these feedbacks using counterfactual measures, we will isolate the first piece,  $\Omega_1 \rightarrow \Omega_2$  (which was not active in Example 3, reproduced in Figure 9 (a), because  $c_2 = 0$  in that case). Here, we fix  $c_1 = 1.0$  and vary  $c_2$ . For the counterfactual, we no longer compare with an independent  $\Omega_1$  Rössler system (i.e. both  $c_1 = 0$  and  $c_2 = 0$ ). Instead, we compare orbits of  $\Omega_1$  in the fully coupled system with orbits from an asymmetrically-coupled system with no feedback, i.e.  $c_1 \neq 0$  and  $c_2 = 0$ .

This measure as a function of  $c_2$  is shown in Figure 9 (b). In the fully coupled case, the dependence on the coupling constant  $c_2$  does not saturate in the same ‘‘weak coupling’’ regime as in Figure 9 (a). Note also that the magnitude of the causal measures in (b) are systematically lower than in (a), as we would expect given that the causal effects in (b) are mediated through  $\Omega_2$ . Unlike the asymmetrically-coupled case, the inclusion of feedbacks prevents the orbits from converging with increased coupling strength—in this case the coupling  $c_2$  from  $\Omega_1$  to  $\Omega_2$ . This result again emphasizes the need to consider nonlinear systems holistically, even when there is linear coupling and weak nonlinearity.

## Appendix C: Proofs

### 1. Proof of Theorem II.1

**Theorem.** *Let  $\mathcal{F}$  be a RKHS, and  $\mathcal{K}^t$  satisfy that  $\mathcal{K}^t f \in \mathcal{F}$  for all  $f \in \mathcal{F}$  ( $\mathcal{K}^t : \mathcal{F} \rightarrow \mathcal{F}$ ). Then  $\mathcal{K}^t$  is bounded (continuous).*

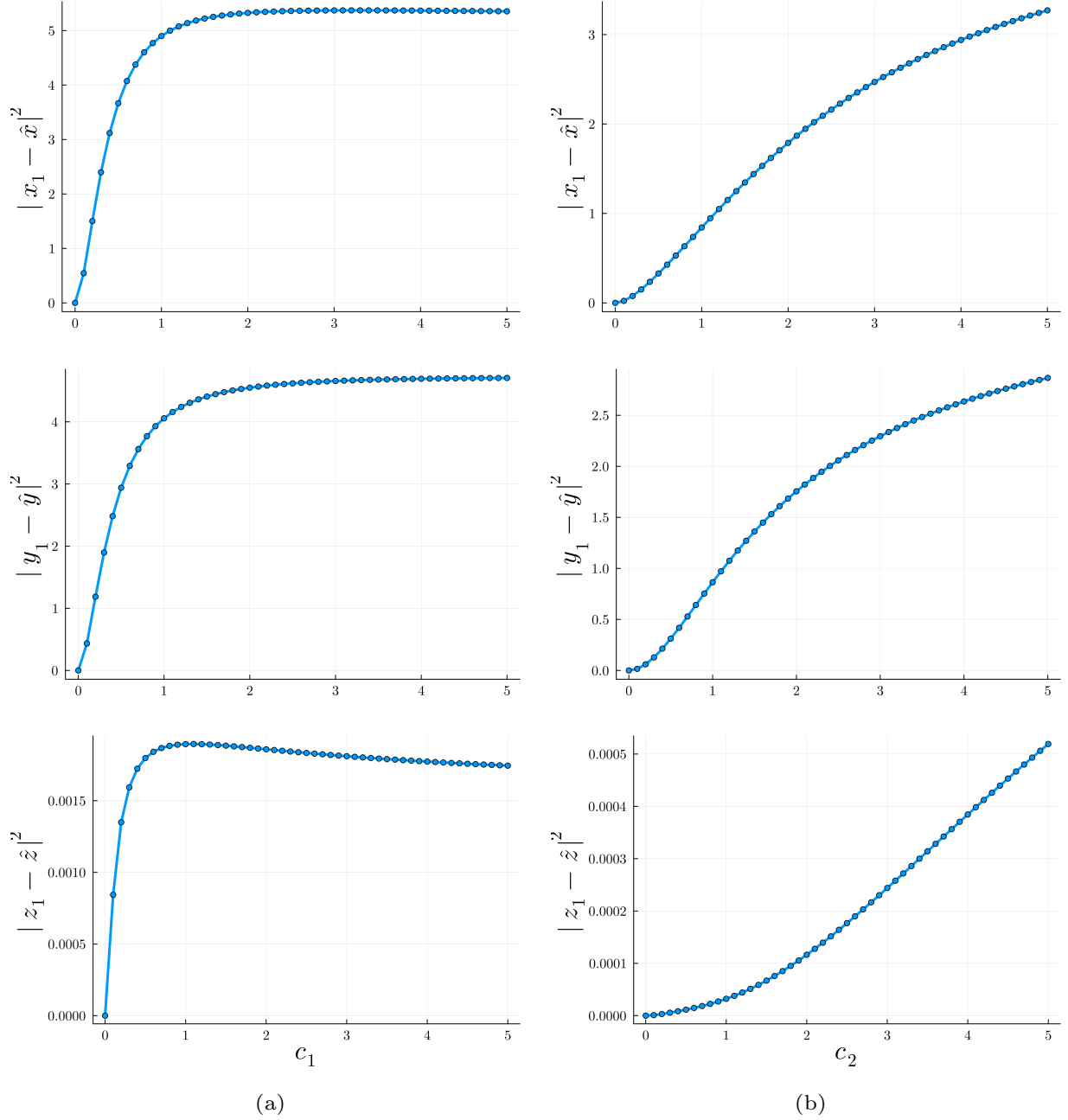


FIG. 9. Some causal phenomenology of the coupled Rössler oscillator system using a counterfactual causality measure. Column (a) shows causality from an asymmetrical system with  $\Omega_2 \rightarrow \Omega_1$  and  $\Omega_1 \not\rightarrow \Omega_2$ . Column (b) shows similar causality measures for the fully-coupled system  $\Omega_2 \rightarrow \Omega_1$  and  $\Omega_1 \rightarrow \Omega_2$ .

*Proof.* By the closed graph theorem,  $\mathcal{K}^t$  is continuous (bounded) if and only if the graph

$$\Gamma(\mathcal{K}^t) := \{(f, \mathcal{K}^t f) : f \in \mathcal{F}\} \subset \mathcal{F} \times \mathcal{F}$$

is closed inside  $\mathcal{F} \times \mathcal{F}$ . Equivalently, the graph is closed if and only if  $f_i \rightarrow 0$ , and  $\mathcal{K}^t f_i \rightarrow g$ , then it

must be the case that  $g = 0$ . Suppose that  $f_i \rightarrow 0$  in  $\mathcal{F}$ . Then for each  $\omega \in \Omega$

$$\mathcal{K}^t f_i(\omega) = f_i(\Phi^t(\omega)) = E_{\Phi^t(\omega)}(f_i)$$

where  $E_x$  is the evaluation functional at  $x \in \Omega$ . No-

tice then that

$$|K^t f_i(\omega)| = |E_{\Phi^t(\omega)}(f_i)| \leq \|E_{\Phi^t(\omega)}\| \|f_i\|_{\mathcal{F}} \rightarrow 0.$$

Hence,  $\mathcal{K}^t f_i(\omega) \rightarrow 0$  point-wise. Now by assumption,  $\mathcal{K}^t f_i \rightarrow g$  in  $\mathcal{F}$ , and hence,  $\mathcal{K}^t f_i \rightarrow g$  point-wise as well. Therefore,  $g(\omega) = 0$  for all  $\omega$ , so that  $g = 0$ , proving the result.  $\square$

## 2. Proof of Lemma III.1

**Lemma.** *Let  $\Omega = \Omega_1 \times \dots \times \Omega_L$ ,  $K_i$ ,  $K$  and  $\mathcal{F}$  be as above. For each  $X \subset \{1, 2, \dots, L\}$ , we have that  $\mathcal{F}_X$  is a closed subspaces in  $\mathcal{F}$ .*

*Proof.* Clearly  $\mathcal{F}_X$  is a subspace of  $\mathcal{F}$ ; it suffices to show it is closed. Suppose that  $(f_n) \subset \mathcal{F}_X$  converges to  $f$ . Then for all  $x \in \Omega_X$  and  $a, b \in \Omega_{X^c}$ , we have

$$\langle f_n, k_{x,a} \rangle = f_n(x, a) = f_n(x, b) = \langle f_n, k_{x,b} \rangle$$

Hence, we have

$$\begin{aligned} |f(x, a) - f(x, b)| &= |\langle f, k_{x,a} \rangle - \langle f, k_{x,b} \rangle| \\ &= \lim_{n \rightarrow \infty} |\langle f_n, k_{x,a} \rangle - \langle f_n, k_{x,b} \rangle| \\ &= 0 \end{aligned}$$

Thus,  $f \in \mathcal{F}_X$ .  $\square$

## 3. Proof of Proposition III.1

**Proposition.** *Let  $X \subset \{1, 2, \dots, L\}$ , and  $K_i$ ,  $\mathcal{F}_X$  be as above. Define the kernel function  $K_X : \Omega \times \Omega \rightarrow \mathbb{C}$  by*

$$K_X(\omega', \omega) := \prod_{j \in X} K_j(\omega'_j, \omega_j)$$

for all  $\omega, \omega' \in \Omega$ . Define the functions  $k_{X,\omega} : \Omega \rightarrow \mathbb{C}$  by  $k_{X,\omega}(\omega') = K_X(\omega', \omega)$ . Then

$$\mathcal{F}_X = \overline{\text{span}_{\omega \in \Omega} \{k_{X,\omega}\}}$$

*Proof.* Let  $\mathbb{1}_i$  denote the identity function  $\mathbb{1}_i(\omega_i) = 1$  on  $\Omega_i$ . By assumption,  $\mathbb{1}_i \in \mathcal{F}_i$  for each  $i$ . Note that  $k_{X,\omega}$  has the form  $k_{X,\omega} = (\otimes_{j \in X} K_{\omega_j}) \otimes (\otimes_{i \in X^c} \mathbb{1}_i)$ .

Indeed, for all  $\omega' \in \Omega$ , we have

$$\begin{aligned} K_{X,\omega}(\omega') &= \prod_{j \in X} K_j(\omega'_j, \omega_j) \\ &= \otimes_{j \in X} k_{\omega_j}(\omega'_j) \\ &= [\otimes_{j \in X} k_{\omega_j}(\omega'_j)] [\otimes_{i \in X^c} \mathbb{1}_i(\omega'_i)] \\ &= (\otimes_{j \in X} K_{\omega_j}) \otimes (\otimes_{i \in X^c} \mathbb{1}_i)(\omega') \end{aligned}$$

From the form  $k_{X,\omega} = (\otimes_{j \in X} K_{\omega_j}) \otimes (\otimes_{i \in X^c} \mathbb{1}_i)$ , we see that  $k_{X,\omega}$  is constant on  $\Omega_{X^c}$ . That is,  $k_{X,\omega} \in \mathcal{F}_X$ . Furthermore, we have that for each  $j$  that  $\overline{\text{span}}\{k_{\omega_j}\} = \mathcal{F}_j$ . Using the fact that  $\mathbb{1}_j \in \mathcal{F}_j$  for each  $j$ , we then get that  $\overline{\text{span}_{\omega \in \Omega} \{k_{X,\omega}\}} = \mathcal{F}_X$ .  $\square$

## 4. Proof of Theorem III.2

**Theorem.** *Dynamical causal influence and Koopman causal influence are equivalent,*

$$\Omega_C \xrightarrow{\mathcal{K}} \Omega_E \iff \Omega_C \xrightarrow{t} \Omega_E$$

Correspondingly,

$$\Omega_C \not\xrightarrow{\mathcal{K}} \Omega_E \iff \Omega_C \not\xrightarrow{t} \Omega_E$$

*Proof.* We will prove  $\Omega_C \not\xrightarrow{\mathcal{K}} \Omega_E \iff \Omega_C \not\xrightarrow{t} \Omega_E$ . Let  $\omega \in \Omega$ . Consider the functions  $k_{E,\omega} \in \mathcal{F}_E$  from Proposition III.1. Note that if  $\omega = [\omega_C \ \omega_E \ \omega_R]^\top \in \Omega$  then we have

$$k_{E,\omega}(\Phi^t([\omega_C \ \omega_E \ \omega_R]^\top)) = \mathcal{K}^t k_{E,\omega}([\omega_C \ \omega_E \ \omega_R]^\top) \quad (\text{C1})$$

By definition,  $\Omega_C \not\xrightarrow{t} \Omega_E$  if and only if  $\Phi^t([\omega_C \ \omega_E \ \omega_R]^\top)$  does not depend on  $\omega_C$ . From Eqn. C1, this happens if and only if the functions  $\mathcal{K}^t k_{E,\omega}$  do not depend on  $\omega_C$ . That happens if and only if  $\mathcal{K}^t k_{E,\omega} \in \mathcal{F}_{E,R}$ . By the linearity of the Koopman operator, we have that for all  $f \in \text{span}\{k_{E,\omega}\}$ , we get that  $\Omega_C \not\xrightarrow{t} \Omega_E$  if and only if  $\mathcal{K}^t f \in \mathcal{F}_{E,R}$ . From Theorem II.1,  $\mathcal{K}^t$  is a bounded operator. It follows from the boundedness of the Koopman operator that by passing to limits, we get  $\Omega_C \not\xrightarrow{t} \Omega_E$  if and only if  $\mathcal{K}^t f \in \mathcal{F}_{E,R}$  for all  $f \in \overline{\text{span}}\{k_{E,\omega}\}$ . However Proposition III.1 states that  $\overline{\text{span}}\{k_{E,\omega}\} = \mathcal{F}_E$ . Therefore, we get  $\Omega_C \not\xrightarrow{t} \Omega_E$  if and only if  $\mathcal{K}^t f \in \mathcal{F}_{E,R}$  for all  $f \in \mathcal{F}_E$ , which is the definition of  $\Omega_C \not\xrightarrow{\mathcal{K}} \Omega_E$ .  $\square$